



UNIVERSITÀ DEGLI STUDI DI PADOVA

**DIPARTIMENTO DI SCIENZE CHIMICHE
CORSO DI LAUREA MAGISTRALE IN CHIMICA**

TESI DI LAUREA MAGISTRALE

Metal free bidimensional catalysts for selective oxidation reactions

Relatore: Prof. Stefano Agnoli

Controrelatore: Prof. Manuel Orlandi

Laureando: Giorgio Lazzari

A. A. 2022/2023

Index

CHAPTER 1	1
PURPOSE OF THIS WORK	1
CHAPTER 2	5
STATE OF THE ART	5
2.1. GRAPHENE.....	5
2.1.1. FLUOROGRAPHENE	9
2.1.2. GO, GA AND GAA.....	10
2.2. GRAPHENE DERIVATIVES FOR CARBOCATALYSIS.....	12
2.2.1. OXIDATION REACTIONS	14
2.2.2. THIOETHER OXIDATION	16
2.2.3. HYDROGEN PEROXIDE DISPROPORTIONATION.....	18
CHAPTER 3	21
RESULTS AND DISCUSSION	21
3.1. SYNTHESIS OF GAA	21
3.2. CHARACTERIZATIONS.....	22
3.2.1. X-RAY PHOTOEMISSION SPECTROSCOPY.....	23
3.2.2. THERMAL ELEMENTAL ANALYSIS	25
3.2.3. FOURIER-TRANSFORM INFRARED SPECTROSCOPY.....	26
3.2.4. SOLID-STATE ¹³ C NUCLEAR MAGNETIC RESONANCE	28
3.2.5. THERMOGRAVIMETRY	29
3.2.6. X-RAY DIFFRACTION	30

3.2.7. Z-POTENTIAL	31
3.2.8. TRANSMISSION ELECTRON MICROSCOPY	32
CHAPTER 4.....	35
CATALYTIC TESTS	35
4.1. THIOANISOLE OXIDATION	35
4.2. HYDROGEN PEROXIDE DISPROPORTIONATION.....	46
CHAPTER 5.....	53
CONCLUSIONS	53
CHAPTER 6.....	57
EXPERIMENTAL SECTION.....	57
6.1. SYNTHESIS OF GAA	57
6.2. BASE AND ACID TREATMENT OF GAA	58
6.3. PHYSICOCHEMICAL CHARACTERIZATIONS	58
6.4. THIOETHER OXIDATION	59
6.5. RECYCLING OF GAA	59
6.6. GENERAL PROCEDURE FOR DETERMINING HYDROGEN PEROXIDE CONCENTRATION VIA UV-VIS ABSORBANCE OF TITANYL SULPHATE COMPLEX	60
6.7. ANALYSIS OF OXYGEN EVOLUTION USING A NEOFOX OXYGEN PROBE.....	60
6.8. ADDITIONAL NMR SPECTRA	61
BIBLIOGRAPHY	71

Chapter 1

Purpose of this work

In the current context of climate change, it seems evident how global warming has already given rise to a number of environmental challenges, which will inevitably become more serious as the ongoing trend continues. Catalysis could be a powerful tool in this situation to build a more sustainable future. In recent decades, the scientific community has seen a rise in concern for sustainability as a means of achieving both environmental and economic objectives. The most illustrative example in this field is the 12-point listing of Green Chemistry edited by Paul Anastas and John Warner in 1998.¹ These are 12 principles that serve as a guiding framework for the design of new chemical products and processes. This new sustainable and environmentally friendly view of chemistry encompasses also the use of catalysis as one of the most effective ways to reduce the amount of waste produced by synthesis processes, compared to the traditional use of stoichiometric reagents. Furthermore, catalysis could help improve the efficiency of reactions by reducing the energy input required, increasing product selectivity, and providing unconventional solutions to traditional chemical challenges. The two major approaches in the field are divided into homogeneous catalysis, where the catalyst is present inside the reaction vessel in the same phase as the substrate, and heterogeneous catalysis, where it is present in a different phase, typically solid.² A good catalyst requires high activity and selectivity, stability for prolonged use, and its

design should aim for a low environmental impact in its synthesis, use, and disposal. Homogeneous, soluble metal complexes are widely used for their high activity and selectivity in several transformations. Still, they present downsides consisting of poor stability and a generally difficult recovery, which is extremely cost-ineffective in terms of time and energy consumption. One solution to such a significant problem could be the use of non-conventional solvents in multiphase homogeneous catalysis, as the use of supercritical fluids or ionic liquids.² A second, more convenient solution could be heterogenization, which consists of immobilizing the catalytic site of the molecule on solid carriers. Solid heterogeneous catalysis comes with some significant advantages, such as ease of recovery through straightforward processes as filtration or centrifugation, allowing for a more efficient and economic recycling of the catalyst. However, the main drawback of such approach is a generally lower activity and selectivity caused by a reduced number and structural variety of active sites available, which is directly related to the amount of surface area exposed to the ambient reaction. In fact, most of the currently industrialized heterogeneous catalysts consist of porous solids with a large surface area hosting deposited or grown catalytic functions.³ While pore dimensions and shape selectivity can modulate the catalytic behaviour of the solid, there are several factors that could drastically reduce the availability of such pores, from the carbonaceous deposition of coke on catalytic solids to ion blocking of zeolites. One way to increase the surface area is to transition from three-dimensional materials like conventional solids to two-dimensional ones. It has been calculated that a single graphene oxide sheet can achieve a specific surface area as high as $2630 \text{ m}^2/\text{g}$ ⁴, while those of common tri-dimensional catalysts reach at most $1000 \text{ m}^2/\text{g}$ ³. It has to be specified that such theoretic value refers to an isolated defect-free graphene oxide sheet, therefore it will be likely impossible to synthesize a stable

material presenting such properties, due to inevitable aggregation phenomena. Another pressing issue faced nowadays is the shortage of resources, particularly from a metal perspective. Examples of this are the rare earth export restrictions from China, and the recent listing by the EU of more and more metals and metalloids as critical raw materials. The latest list composed by the EU Directorate-General for Internal Market, Industry, Entrepreneurship and SMEs on 16 March 2023 includes the platinum group metals, rare-earth elements, aluminium (bauxite), cobalt, gallium, and many other materials which catalysis relies upon.⁵ As a consequence, most of the commonly used metals will also experience a heavy price spike in the foreseeable future. It is therefore essential to reduce the amount of critical raw materials used in chemistry and related fields. In recent years, new and promising techniques have been developed to maximize the surface area of metal catalysts, from nanoparticles down to single-atom catalysis. The exacerbation of this new trend of metal-saving eventually envisions metal-free carbon-based materials. As indicated by their name, these catalysts do not require any metal to work and are based solely on simple functional groups. The first material of this kind that garnered the attention of chemists is undoubtedly graphene, due to its high specific surface area and interesting chemical and electronic properties. As stated before, alongside the catalytic behaviour of a catalyst, it is important to consider how it can be synthesized and disposed of in the simplest, greenest, and most sustainable way. Conventional metal catalysts are synthesized using highly pollutant methodologies that require the use of unsustainable reagents, strong acids, bases, or hazardous materials, etc., or high-energy inputs like solid-state reactions.

In the present work, we optimised an innovative low-temperature synthesis of a new bi-dimensional graphene-based material. The first part of the thesis concerns the synthesis and characterization of graphene acetic acid (GAA). This material was

synthesized using mild conditions and low impact reagents like fluorographite and diethylmalonate. While dimethylformamide is an optimal solvent for the reaction, anisole was tested as a greener and non-toxic alternative. Comparable results in terms of yield and functionalization degree were observed.

The second part of the thesis focuses on the catalytic studies conducted on GAA. The material was first employed in the oxidation of thioethers to sulfoxides, observing a significant lowering of both the temperature and time required by the uncatalyzed reaction. Based on the reported strong peroxidase activity, a pseudo-catalase activity in the hydrogen peroxide disproportionation reaction was then explored. In this latter case, the study did not produce the expected results, with the material not working as a catalyst for such reaction.

Chapter 2

State of the art

2.1. Graphene

Graphene is a two-dimensional sheet of sp^2 hybridized carbon atoms (Fig. 2.1) and can be considered the precursor of all other sp^2 carbon allotropes. It essentially serves as the building block for carbon nanotubes and fullerenes (rolled-up graphene sheets) and graphite (stacked graphene sheets). The first isolation and characterization of pristine single-layer graphene occurred in 2004 by A. Geim and K. Novoselov, by use of their "Scotch tape method," which involved micromechanical exfoliation of highly oriented pyrolytic graphite. This discovery opened a new world in materials science. Prior to this, it was commonly believed that two-dimensional materials were thermodynamically unstable at finite temperatures.⁶

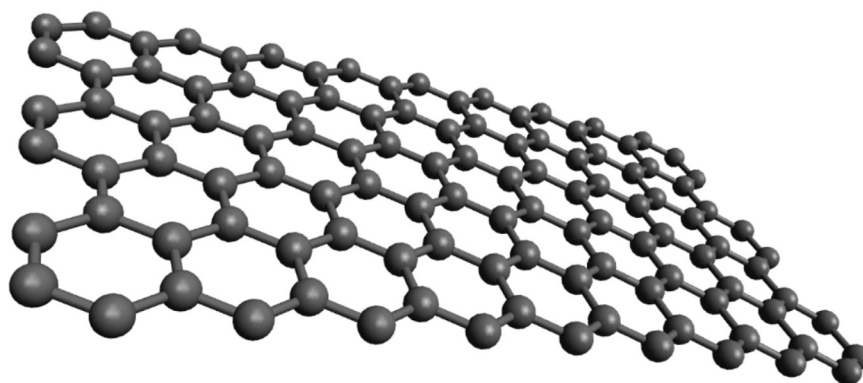


Figure 2.1: Ball and stick model of a pristine graphene sheet.

The structure of graphene, composed of both strong C-C sigma bonds and a delocalized π orbital system, imparts graphene with various interesting physical properties. These properties range from strong anisotropy in its electrical characteristics to outstanding electrical conductivity within the plane ($4000 \text{ Wm}^{-1}\text{K}^{-1}$), high thermal conductivity ($3000 \text{ Wm}^{-1}\text{K}^{-1}$), and high mechanical stiffness (1060 GPa).⁷ All these intriguing properties have made graphene and its derivatives extremely interesting for various potential applications, including data storage, high-speed electronics, LCD, and OLED, to name just a few. During this project, we focused on the potential catalytic applications of graphene derivatives for fine chemical synthesis. One of the most significant challenges in effectively using single-layer graphene is its tendency to aggregate. In fact, the large sp^2 domains tend to interact with each other through π - π interactions, forming a graphite structure that is far less soluble. The primary solution to this problem is to synthesize graphene derivatives with more favourable interactions with the solvent. One of the earliest graphene derivatives is Graphene Oxide, which is a highly oxygenated graphene sheet. Graphene oxide bears various types of defects, such as hydroxyl and epoxide functional groups on its plane, and carbonyl and carboxyl groups at the sheet edges, making it far more hydrophilic and easily dispersible in water. Furthermore, graphene oxide can be produced on a large scale using the "Hummers method" (Fig. 2.2), developed by William Hummers in the late 1950s to strip sheets from a graphite source, albeit this method involves the use of strong oxidizing agents and acids (K_2MnO_4 , NaNO_3 and concentrated H_2SO_4).⁸

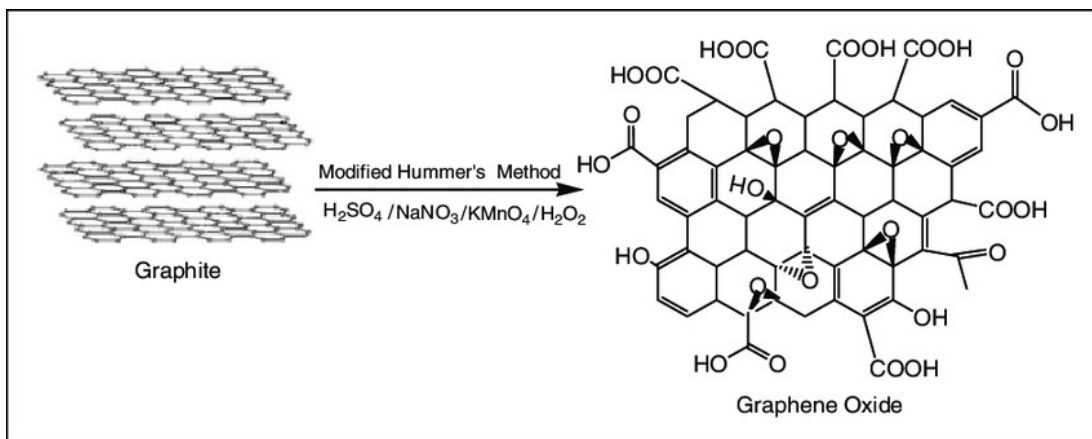


Figure 1.2: Modified Hummers method to synthesize GO starting from graphite. Adapted by Nafees et al.⁹

The obtained graphene oxide exhibits lower electron conductivity properties due to the presence of defects that reduce conjugation. Therefore, a second reduction treatment is necessary to restore the sp^2 network and improve conductivity, while retaining the hydrophilicity and dispersion capacity caused by the remaining oxidized groups. Over the years, a significant number of reductants have been studied for synthesizing graphene oxide, but the main challenge lies in the heterogeneity of the results. Different oxidants lead to varying physical properties. Additionally, many of these reduction processes involve the use of strong and potentially toxic reagents under harsh conditions, arising environmental concerns.¹⁰ Apart from the most common synthetic routes (Fig. 2.3), there are other, less-utilized possibilities, such as chemical vapor deposition, liquid-phase exfoliation, and growth on SiC, each with different costs, environmental impacts, and material outcomes.¹¹

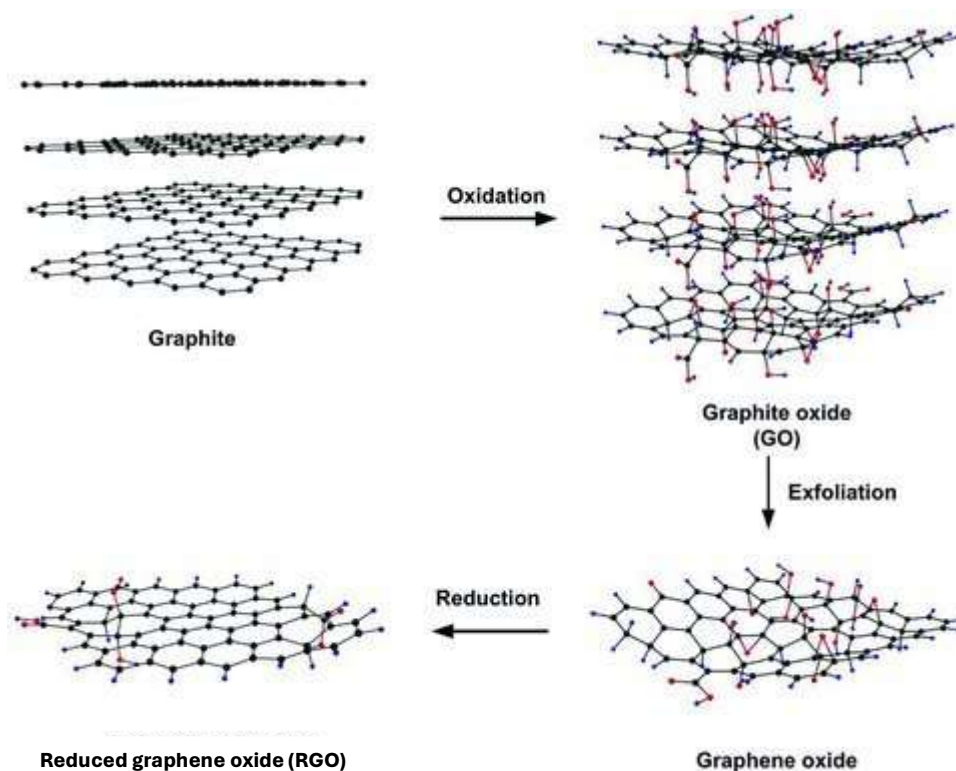


Figure 2.3: Graphene oxide and reduced graphene oxide sample structures. Adapted from Bai et al.¹²

When it comes to the functionalization of graphene, different strategies are available.¹³ Substitutional doping involves replacing carbon atoms from the hexagonal honeycomb lattice of graphene with heteroatoms, most often nitrogen¹⁴ or boron.¹⁵ Non-covalent functionalization exploits π interactions with different ligands to increase solubility without modifying the electronic network. However, the most important functionalization method involves covalently bonding different groups to the graphene sheet. This can be achieved in several ways, a basic one being the attachment of free radicals to sp^2 carbon atoms. However, this reaction is often expensive and uses unstable reagents like diazonium salts.¹⁶ A more favourable functionalization strategy can be carried out by exploiting the different heteroatoms present as defects on graphene, such as oxygen groups like alcohol or carboxylic acid, for esterification or amidation reactions. A new and promising approach to obtain functionalized graphene derivatives comes from fluorographite chemistry.

2.1.1. Fluorographene

Fluorographene is a stoichiometric monolayer compound with a C_1F_1 composition (Fig. 2.4). Despite the C-F bond being one of the strongest, with a bond dissociation energy (BDE) of 108-130 kcal mol⁻¹,¹⁷ it exhibits strong electrophilic behaviour. This is likely due to the partial ionic character of the bond or structural defects.¹⁸

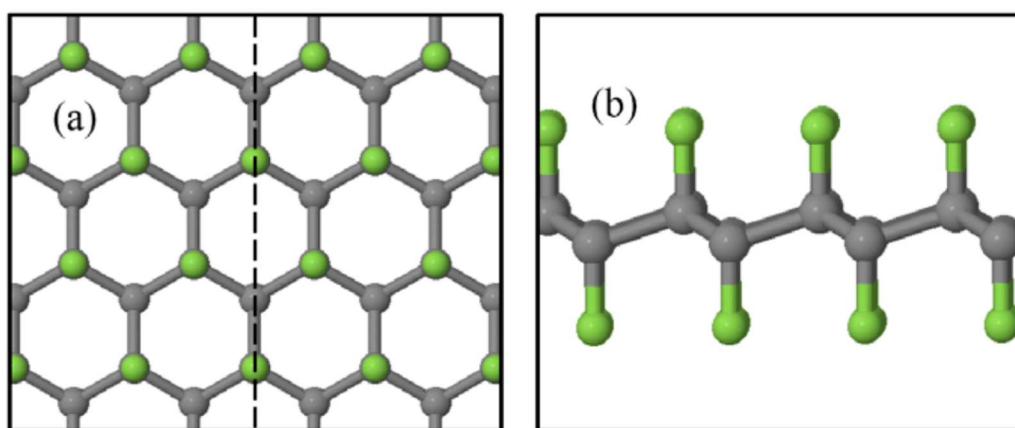


Figure 2.2: a) Top-down view of FG; b) side view of the chair conformation of FG. Adapted from Yang, L.; Liang Y.¹⁹

Defluorination of fluorographene can be achieved through chemical means, such as sonication in a strong polar solvent,²⁰ or thermally.²¹ Sonication is the more convenient option in terms of yield and sustainability. The primary advantage of the former method is that it can occur simultaneously with a nucleophilic substitution, allowing for the formation of graphene derivatives in absence of fluorine. It has been suggested that a bimolecular nucleophilic substitution (S_N2) is the preferred mechanism for the substitution of fluorine atoms.²² Various reactions can be employed to obtain graphene derivatives, including Grignard,²³ Bingel-Hirsch,²⁴ photo Diels-Alder,²⁵ Sonogashira,²⁶ and others involving common nucleophiles like cyanide.²⁷ As mentioned earlier, this reaction can occur under relatively mild conditions with a relatively high level of reproducibility, making it essential for synthesizing materials with stable product properties. This contrasts with the standard synthetic pathway for

graphene oxide, which is highly unreproducible and requires strong oxidizing agents and conditions. There are two major approaches to synthesize fluorographene. The first involves the mechanical exfoliation of fluorographite,²¹ a material known since 1934²⁸ and widely used as an industrial lubricant. The second method is direct fluorination of graphene, for example, using XeF₂.²⁹ A promising new synthetic route could involve using a fluorinated polymer as a source of fluorine radicals to directly fluorinate a graphene sheet, as proposed by Lee et al.³⁰ This method, if adapted to different fluorinated polymers, such as polytetrafluoroethylene, could help address the disposal challenges associated with per- and polyfluoroalkyl substances (PFAS) due to their high stability.³¹

2.1.2. GO, GA and GAA

When it comes to functionalizing graphene oxide (GO), the most commonly used group is carboxylic acid, which is present as a defect on graphene oxide.¹³ This defect has been exploited to synthesize various graphene derivatives (Fig. 2.5). A series of methods has been studied to enhance the functionalization of acid groups on graphene sheets. The term "graphene acid" was first coined in 2016 when Sofer et al. obtained a pseudo-stoichiometric material known as GA, through a sequential oxidation process.³² This process achieved a high concentration of carboxylic acid groups on the graphene sheet, up to 30 wt%. However, it resulted in the alteration of the physical properties of graphene due to significant structural modifications. The synthesized GA exhibited a wrinkled 3D structure due to strong hydrogen bonding between different sheets, leading to material aggregation. Additionally, high-resolution X-ray photoelectron spectra of GA lacked the peak corresponding to the C=C double bond, indicating a different structure due to the high degree of functionalization.

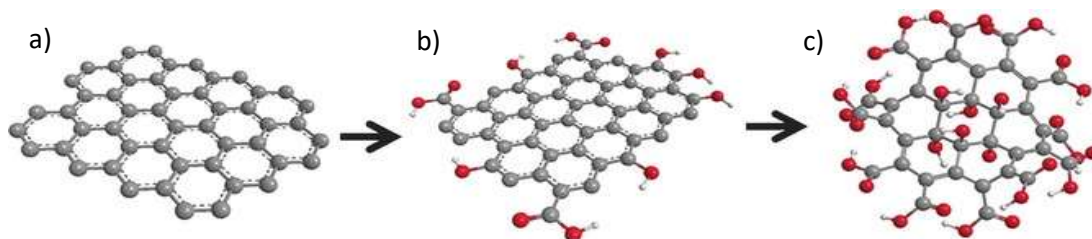


Figure 2.3: a) Graphene, b) graphene oxide and c) graphene acid structure sample. Adapted from Jankovsky O.³²

Another drawback of this synthetic method is the low yield, approximately 30% of the initial GO, which is attributed to the decomposition of highly oxidized areas into CO₂. Another group reported the synthesis of graphene acid with a high concentration of functional groups by starting from fluorographite.³³ The synthesis involves two distinct steps (Fig. 2.6): the first consists in a nucleophilic substitution with NaCN to obtain cyanographene with 24 wt% of cyano functional groups, and the second involves hydrolysis with 20% nitric acid. This leads to the complete conversion of cyano groups to carboxylic acid, with only a slight decrease in the degree of functionalization.

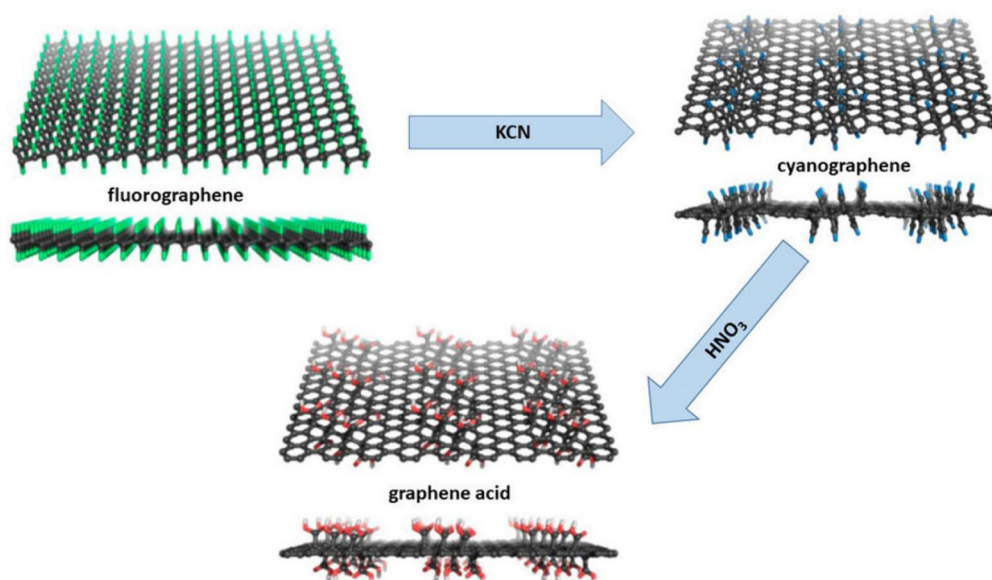


Figure 2.4: Schematics of the synthetic procedure for cyanographene and GA employed by Otyepka et al.³³ F: green; N: blue; O: red; H: white.³⁴

Besides having a higher degree of functionalization, graphene acid (GA) differs from graphene oxide (GO) in other important aspects, foremost in the location of these defect points. In GO, carboxylic functions are primarily located at the edges of the flakes, while the basal plane is mainly covered with hydroxyl and epoxide groups, following the widely accepted Lerf-Klinowski model.³⁵ In contrast, GA features carboxylic functions homogeneously distributed across the surface of the flakes. Furthermore, the physical properties of GA differ significantly from those of GO. For example, it exhibits a higher conductivity than GO, with a sheet resistivity of $6800 \Omega \text{ sq}^{-1}$ for GA compared to $2174 \times 106 \Omega \text{ sq}^{-1}$ for GO.³³ This increased conductivity is maintained even with a high degree of functionalization compared to other graphene derivatives. This high level of functionalization opens numerous possibilities for further functionalization. Otyepka et al. successfully explored covalent binding through amide bonds,³³ but other possibilities such as esterification remain to be investigated. Lastly, we want to mention the Acid Graphene Oxide (AGO) synthesized by Abdi et al.³⁶ since it was used as benchmark to be compared with the catalytic behaviour of Graphene Acetic Acid (GAA), the graphene-based material studied during this project. AGO is a particular enriched graphene oxide obtained by further but blander oxidation of graphene oxide with hydrogen peroxide. This material, instead of losing most of its electrical properties due to the overoxidation, resulting in the loss of its π system, retains most of the properties of graphene-based materials.

2.2. Graphene derivatives for carbocatalysis

Carbocatalysis involves the use of catalysts composed almost exclusively of carbon, with the aim of reducing the amount of metals used in chemical processes. To qualify as a carbocatalyst, the active part of it must consist solely of carbon derivatives without

any metals. This excludes the new types of materials used in single-atom catalysts or nanoparticle catalysts. In addition to metal saving, carbon catalysts are often more cost-effective. Carbon-based materials such as graphene, nanotubes, and fullerenes are typically cheaper compared to precious metals like palladium and platinum, which have seen a significant increase in price due to their scarcity in recent decades.³⁷ Moreover, many metal-based catalysts can be harmful to the environment and pose serious risks to human health, both during their use and, more frequently, during their synthesis and disposal. In contrast, carbon-based materials can often be synthesized under mild conditions using common reagents, and their disposal is straightforward. Another significant advantage of carbocatalysis is its intrinsic heterogeneity. Unlike organocatalysis, where small organic molecules are used under homogeneous conditions to catalyse reactions, carbon-based materials are solid and can be easily recovered after each cycle. This is a major advantage over normal metal-based catalysis, which often relies on metal complexes in a homogeneous state, making difficult their recovery. Bielawski's group pioneered the investigation of the catalytic behaviour of graphene derivatives.³⁸ They used graphite oxide (GO) to convert alcohols, alkenes, and alkynes into aldehydes and ketones. Unfortunately, to achieve good conversion rates, they had to use a high catalyst loading, approximately 200 wt% relative to the weight of the reactant.

Furthermore, later studies from other groups indicated that the reaction could possibly be not catalytic, but rather stoichiometric.³⁹ In fact, GO used as a catalyst for the benzyl alcohol oxidation acted instead as an oxidant and lost up to 73% of its oxygen content during the process. For the same reaction, graphene acid (GA) yielded far better results.⁴⁰ GA was used by Agnoli's group in a catalytic amount (5 wt%), and it was proven to retain its catalytic activity for more than 10 cycles. They achieved complete

conversion in just two hours by using nitric acid as a co-catalyst, setting a new standard for carbocatalysis and in specific cases surpassing the performance of noble metal catalysts.³⁴ Through density functional theory (DFT) calculations, it was ascertained that GA selectively binds nitric acid and promotes a series of electron transfer and redox reactions. A similar approach was followed in this work to investigate the catalytic capabilities of GAA (Fig. 2.7), a carbocatalyst for oxidation reaction, which is based on a very similar functional group.

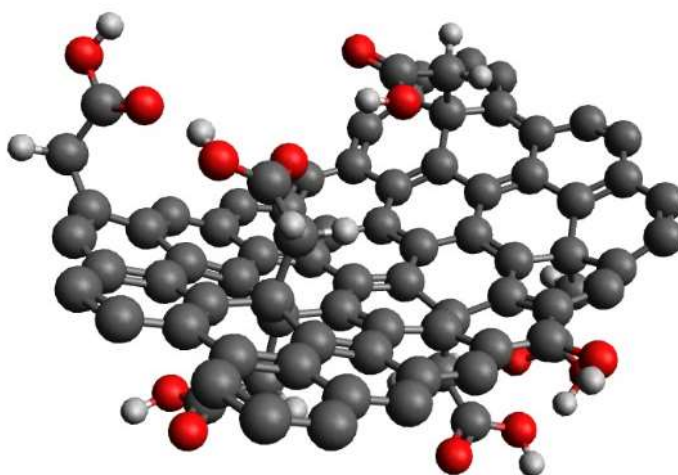


Figure 2.5: Ball and stick representation of Graphene Acetic Acid (GAA).

2.2.1. Oxidation reactions

Oxidation reactions represent a cornerstone of modern synthetic processes, playing an essential role in all fields of chemistry, from the production of bulk chemicals to fine chemicals and pharmaceuticals. It is estimated that approximately one-quarter of all catalytic processes involve partial oxidation reactions.⁴¹ The primary challenge in these reactions lies in product selectivity, as oxidation is an inherently complex process, with multiple parallel reaction pathways leading to unreactive, stable

byproducts. A significant contribution to the sustainability of oxidation reactions involves transitioning to heterogeneous catalysts. Currently, most oxidation processes are carried out using conventional stoichiometric reactants, resulting in the generation of large amounts of waste. Heterogeneous catalysts, for the most part, promote oxidation reactions by facilitating the transfer of oxygen from an oxidant,⁴² often tert-butyl hydroperoxide or hydrogen peroxide, to the substrate. The most commonly used heterogeneous catalysts are inorganic redox materials. Their inorganic nature makes them less susceptible to oxidative degradation compared to most organic counterparts. Various carbonaceous materials have been investigated for their catalytic potential, including activated carbon and carbon fibres. However, their structural complexity and impurities often limit their performance.⁴³ Graphene oxide (GO) has also been tested for its ability to release SO_4^{2-} from potassium peroxymonosulfate, with the goal of catalysing the degradation of organic compounds.⁴⁴ Through different functionalization methods and DFT calculations, it has been revealed that the catalytic functionalities are associated with the carbonyl groups present on the edges of the graphene sheets.⁴⁵ Other carbon nanostructures, such as carbon nanotubes and nanoribbons, have also demonstrated the capability to activate potassium peroxymonosulfate.⁴⁶ Various strategies have been explored to enhance the oxidative properties of carbon nanostructures, from nitrogen doping⁴⁷ to the synthesis of nanocomposite materials.⁴⁸ Since the catalytic activity of carbon materials greatly depends on their nanostructure, it is important to develop straightforward synthetic routes to obtain finely controlled nano systems with high catalytic efficiency. In the context of oxidation reactions and carbocatalysis, the inclusion of an oxidant co-catalyst is necessary. Several options exist, with the most used being peroxymonosulfate (PMS), peroxydisulfate (PDS), hydrogen peroxide (H_2O_2), and

ozone. Despite its abundance, activation of molecular oxygen as an oxidizing agent is not a straightforward step. Ozone is a viable secondary option, but the main drawback of its use lies in its instability, requiring in-situ generation and immediate usage, making it unsuitable for mass storage.⁴⁹ Consequently, the most effective oxidant that a proficient catalyst should aim to activate is hydrogen peroxide, due to the non-toxic nature of its byproduct, water.⁵⁰

2.2.2. Thioether oxidation

Thioethers are a well-known class of organic compounds with diverse applications, ranging from the synthesis of polymers⁵¹ to the creation of chiral ligands for asymmetric catalysis.⁵² However, the most significant and prevalent application of thioethers and their derivatives lies in pharmaceutical synthesis. Sulfoxides, in particular, are widely used in pharmaceuticals as anti-ulcer and anti-acid drugs, such as gastric Proton Pump Inhibitors (PPIs) like omeprazole and esomeprazole (Fig. 2.8). These sulfoxides are considered to be chiral, with the sulphur atom carrying a lone pair of electrons. They adopt a trigonal pyramidal shape due to their tetrahedral electron pair geometry. One of their most important properties is their low racemization rate, with optical purity maintained until temperatures reach approximately 200°C, at which point racemization begins. This characteristic makes them valuable in chiral synthesis of ligands.⁵²



Figure 2.6: Omeprazole (left) and S-omeprazole/esomeprazole (right).

Sulfones, on the other hand, are less commonly used as drugs, with examples like the antibiotic and anti-leprotic dapsone. However, they find wide application as monomers in polymer chemistry, as polysulfones (Fig. 2.9) are a class of high-performance thermoplastics for biocompatible materials.⁵³

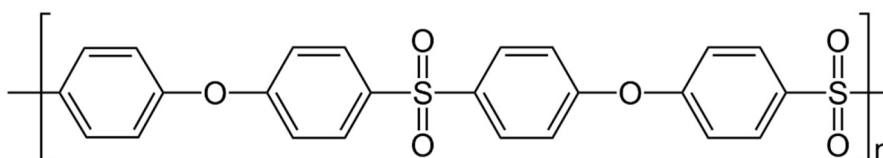


Figure 2.7: An example of aromatic polysulfone, polyethersulfone (PES).

Therefore, the functionalization and oxidation of thioethers are important reactions that have been extensively studied. Various oxidants have been explored for this purpose, including nitric acid, organic peroxides, and heavy metal oxidants.⁵⁴ Among these, hydrogen peroxide stands as green oxidant capable of oxidizing thioethers to sulfoxides and sulfones under high temperatures or with extended reaction times in the absence of a catalyst. However, achieving highly selective oxidation through the sole control of reaction conditions is a challenging task. Lowering the reaction time or temperature is advantageous both in terms of energy and cost savings. Different metal compounds, either homogeneous⁵⁵ and heterogeneous,⁵⁶ have been employed with varying results in terms of conversion and selectivity. While most metal catalysts can expedite the reaction, achieving precise control can be difficult, with many catalysts leading to the oxidation of most thioethers to sulfones. In the field of metal-free catalysis, two major approaches are found in the literature: organocatalysis and carbocatalysis, with the former being homogeneous and the latter heterogeneous. In 2007, Golchoubian and Hosseinpour reported a selective method to convert various thioethers into their respective thiosulfides using an organocatalytic approach.⁵⁷ They utilized glacial acetic acid and a thioether-to-hydrogen peroxide molar ratio of 1/4, achieving full conversion to sulfoxides in 80 minutes at room temperature. On the

other hand, the separation of acetic acid necessitates a second extraction step with dichloromethane. Carbocatalysis is another viable approach, as reported by G. Abdi and colleagues.³⁶ They used a carboxyl-enriched graphene oxide⁵⁸ to catalyse the conversion of thioethers to sulfones, achieving complete conversion using 20 wt% of the catalyst within one hour.

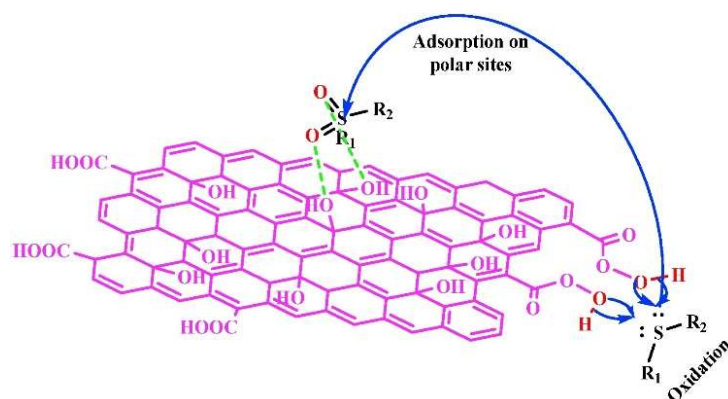


Figure 2.8: Hypothetical mechanism of sulfide oxidation to sulfone with carboxyl enriched rGO. Adapted from Abdi et al.³⁶

The proposed mechanism (Fig. 2.10) involves the concerted oxidation of sulphides to sulfoxides via the formation of intermediate peroxyacids. The lone pairs on the sulphur atom attack the electrophilic oxygens on two adjacent peroxyacids, resulting in the formation of double S=O bonds. The selectivity toward sulfoxides may be attributed to the high concentration of functional groups at the edges of the graphene sheets, leading to the presence of multiple acetic functional groups nearby.

2.2.3. Hydrogen peroxide disproportionation

As stated before, hydrogen peroxide is one of the greenest oxidants available, and it also covers a biological role in living animal organisms. However, its excess can cause serious damage to cells and tissues. The excess of hydrogen peroxide and, in general, reactive oxygen species (ROS) inside the body is referred to as oxidative stress, and it is linked to the onset of various diseases.⁵⁹ Hydrogen peroxide is a by-product of

respiration and an end product of several metabolic reactions, and it can react with the thiol group of cysteine, which is an amino acid contained in most animal proteins.⁶⁰ Cells have developed multiple defences against hydrogen peroxide, with the two major ones being catalase and peroxidase enzymes (Fig. 2.11). Catalase activity involves the decomposition of hydrogen peroxide into water and oxygen, making it essential for controlling ROS concentration. Sometimes the normal catalase activity of the enzymes is insufficient to prevent oxidative stress, for example when external implants or prostheses are introduced. In the case of metal-on-metal prostheses, the cobalt and chromium they contain can enhance the production of ROS⁶¹. In the case of polymeric implants, instead, the excess of naturally occurring ROS species in the body can accelerate the degradation of the material, usually ultra-high molecular weight polyethylene, leading to the deterioration or rejection of the implant and, subsequently, the need for its replacement. Ultimately, ROS accumulation leads to aging of tissues and skin.⁶²⁶³ Most of the catalysts currently used for the decomposition of hydrogen peroxide are metal-based⁶⁴ due to their high activity, but they lack biocompatibility. The development of new carbon-based catalysis, likely to be more compatible, could pave new ways for treating oxidative stress-related diseases.

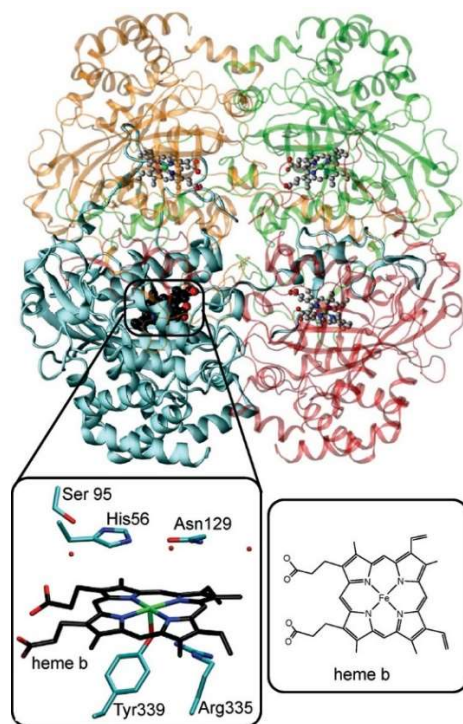


Figure 2.9: Structure of *H. pylori* catalase. Top: cartoon picture of the protein Bottom: heme binding pocket and heme group. Adapted from Alfonso-Prieto M et al.⁶⁵

Chapter 3

Results and discussion

3.1. Synthesis of GAA

The synthesis of graphene acetic acid can be achieved in two simple steps under mild conditions. As stated in the introduction, similar graphene derivatives with acid functionalities have been developed by Otyepka et al.²⁷ Unfortunately, their synthesis required the use of sodium cyanide, which is a very harmful and unsafe chemical. Our goal was to develop a new material with acid functionalities without the use of such reagent. Similarly to Otyepka's work, the starting material was commercial fluorographite (C_1F_1), but we adopted diethyl malonate as a nucleophile instead of cyanide.

Regarding the choice of the solvent, the synthesis was developed using N,N-dimethylformamide (DMF) due to its capability to exfoliate fluorographite and trigger its reductive defluorination. Furthermore, anisole has also been tested as a greener and more sustainable alternative, as established by GSK's guide.⁶⁶ Fluorographite was suspended in the chosen solvent after being dehydrated through three vacuum-nitrogen cycles. This step is necessary to create inert conditions inside the exfoliating site to prevent the presence of nucleophiles that could attach to the fluorographene and reduce the degree of carboxylic functionalization.

The fluorographite was sonicated for 4 hours, a time that was sufficient for the complete exfoliation but not complete defluorination. This process generated some sp^2 domains, resulting in a characteristic dark colour, interrupted by unreacted sp^3 carbon atoms still bonded to fluorine. Then, diethyl malonate was added to the sonicated fluorographite, which was previously deprotonated using potassium carbonate in the same solvent, at 0 °C to prevent self-reaction. The resulting mixture was left to react overnight at 130 °C under magnetic stirring. This led to the complete substitution of the remaining fluorine by the diethyl malonate. The resulting material was washed several times, either with acetone and water, to remove impurities such as unreacted diethyl malonate, fluorides and carbonates.

The second step of the synthesis consists of the acid hydrolysis of the esters, followed by a decarboxylation process. To achieve this, the material was sonicated for 4 hours in water, before adding a few drops of sulfuric acid and allowing the mixture to react at reflux for 24 hours. The mild conditions were sufficient to decarboxylate one of the ester groups of the diethyl malonate, leaving one acid functionality in the material.

The final material was washed again with water and acetone and vacuum dried. To obtain the material as dispersible as possible, a freeze-drying process was carried out.

3.2. Characterizations

The obtained material was characterized using several techniques to assess its chemical composition, retained functionalization, colloidal stability, morphology and to verify the absence of residual fluorine from the substitution synthetic step performed on fluorographene.

3.2.1. X-Ray photoemission spectroscopy

The chemical composition of the material was determined using X-Ray Photoemission Spectroscopy (XPS). To perform this analysis, a thin film of the material was drop-casted onto a copper sample holder and introduced into a custom-designed ultra-high vacuum chamber with a base pressure lower than 10^{-9} mbar. An electron analyser and an Al K α photon source were employed. The obtained spectrum reveals the presence of carbon and oxygen through their respective 1s peaks (Fig. 3.1). According to our expectation, the fluorine peak is absent from the spectrum, indicating the absence of residual fluorine in the material. The remaining observed peak is attributed to the copper sample holder used to support the material.

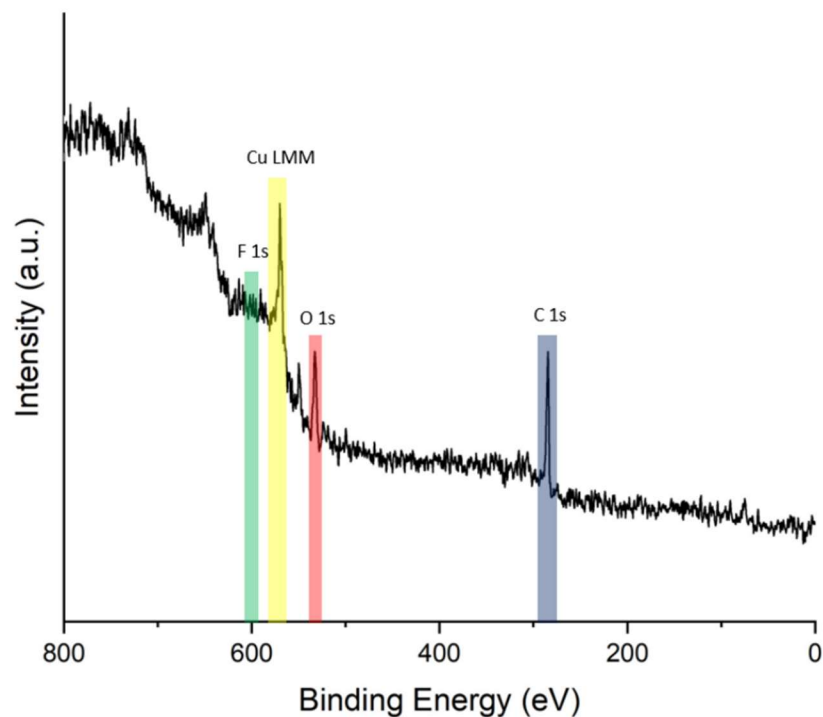


Figure 10: XPS survey spectrum of GAA. From right to the left, C 1s, O 1s, Cu LMM and F 1s peaks expected locations are highlighted respectively in blue, red, yellow and green.

To determine the sample composition, the photoemission intensity of the C 1s and O 1s peaks was normalized using relative sensitivity factors. These factors were calculated based on the Lindau-Yeh photoionization cross sections⁶⁷ and the inelastic

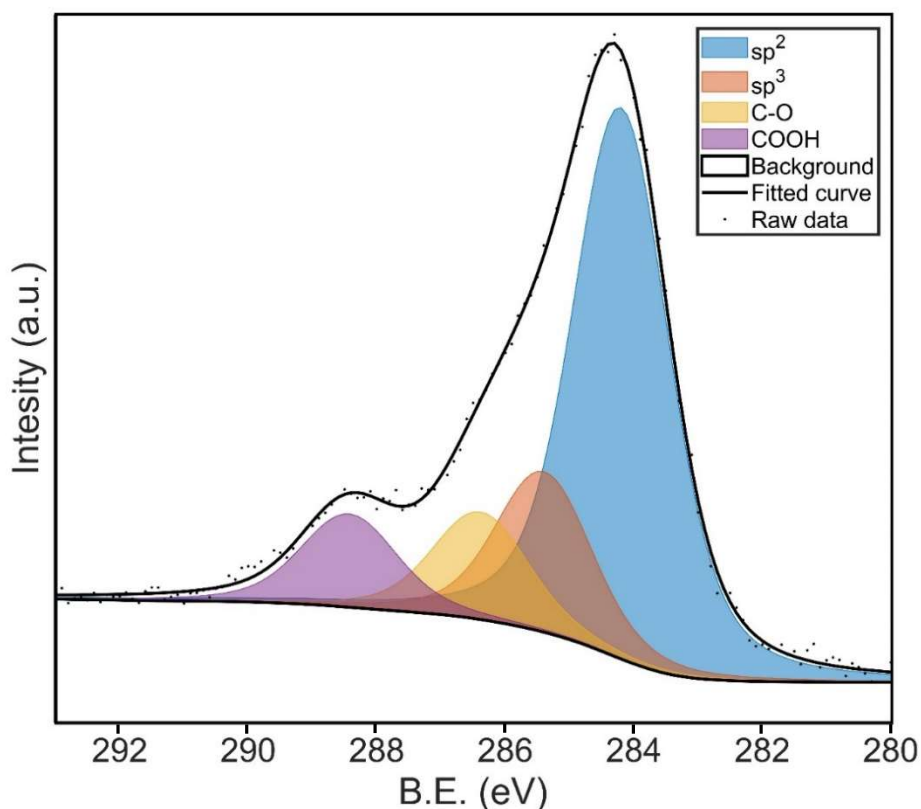
mean free path obtained through the TPP-2M (Tanuma, Powell, and Penn algorithm).⁶⁸

The atomic composition of the sample was found to be 77 at% C and 23 at% O, consistent with our expectations. The separation of the C 1s photoemission line into chemically shifted component allows us to distinguish the various species of carbon atoms present in the material, providing insight into its functionalization (Fig. 3.2).

From the assignment, it can be observed that 10% of carbon atoms exist in the form of carboxylic functions. These results are comparable to other synthetic routes for graphene acid.²⁷ To further confirm the presence of such functions, various techniques have been employed, which are described further on.

In addition, 12% of carbon atoms are singularly bonded to oxygen, which may be attributed to the presence of water in the hygroscopic potassium carbonate or any remnants in the solvent after the vacuum process. To investigate this, another synthesis using anhydrous reagents and solvent could be conducted in future studies.

As anticipated for a graphene-based materials, the majority of carbon atoms are contained within sp^2 domains (60% of the total carbon atoms). Nonetheless, 18% of carbon exists in sp^3 form. This can be attributed to the presence of tetrahedral C atoms in correspondence of nucleophilic substitution sites, and to the methylene bridges connecting the carboxylic functions to graphene. An important piece of information derived from the C 1s deconvolution is the absence of significant features at 291.0 eV binding energy, typical of C-F bonds. This further supports the hypothesis of a complete defluorination of fluorographene, as suggested by the survey XPS spectrum.



	sp^2	sp^3	C-O	O-C=O
B.E. (eV)	284.6 ± 0.2	285.8 ± 0.2	286.8 ± 0.2	288.8 ± 0.2
Amount (%)	60	18	12	10

Figure 3.2: Deconvolution of C 1s photoemission peak in GAA. Assignment given accordingly to the highlighted literature.

3.2.2. Thermal elemental analysis

The thermal elemental analysis of the material has been obtained and is presented in Table 1. As anticipated, the most abundant elements are carbon, oxygen and hydrogen. The small percentage of nitrogen can be attributed to the presence of residual reaction solvent (DMF) within the material. The minor disparities between this analysis and the results obtained from the XPS measurements may be attributed to the presence of copper oxide on the sample holder used in the latter technique, which leads to a slight overestimation of the oxygen percentage. Thermal analysis data can be more accurate regarding the oxygen fraction actually present in the material. Nonetheless, the values

reported in Table 3.1 align with the data obtained from the deconvolution of the carbon 1s photoemission peak.

Table 3.1: Elemental analysis of GAA.

Elements	Mass %
C	70.44
O	26.41
H	2.53
N	0.62

3.2.3. Fourier-transform infrared spectroscopy

An FT-IR spectrum was acquired to verify the presence of carboxylic functionalities. As depicted in Fig. 3.3, C=O and C-O stretching bands are found at 1730 cm^{-1} and 1220 cm^{-1} , respectively, highlighting the effective formation of oxygenated functional groups on the material. Additionally, the presence of both the C=C stretching mode for sp^2 carbon atoms and the C-H stretching mode of sp^3 carbon atoms confirms the presence of both the conjugated system and the methyl groups linking the carboxylic functions to the aromatic domain, respectively. The results of the FT-IR analysis are therefore in agreement with those provided by XPS.

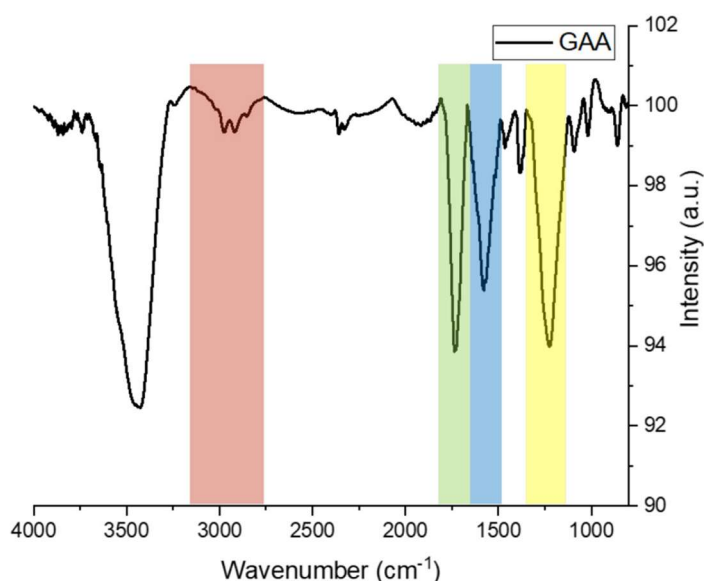


Figure 3.3: GAA in KBr infrared spectrum: C-H stretching at 3000 cm^{-1} (red), C=O stretching at 1730 cm^{-1} (green), aromatic C=C stretching at 1600 cm^{-1} (blue) and C-O stretching at 1220 cm^{-1} (yellow).

To further confirm the presence of carboxylic acids, additional IR spectra were recorded after treatment with 1M NaOH for 1 hour and subsequent acid treatment with 1M HCl (Fig 3.4). The graphs indicate that after treatment with the base, the intensity of the C=O stretching peak at 1730 cm^{-1} consistently decreases, while around 1450 cm^{-1} another peak intensifies. This peak can be attributed to the O-C-O symmetric stretching of the carboxylates formed during the base treatment. These changes revert to their original state after the subsequent acid treatment, confirming the presence of the presumed carboxylic acid groups.

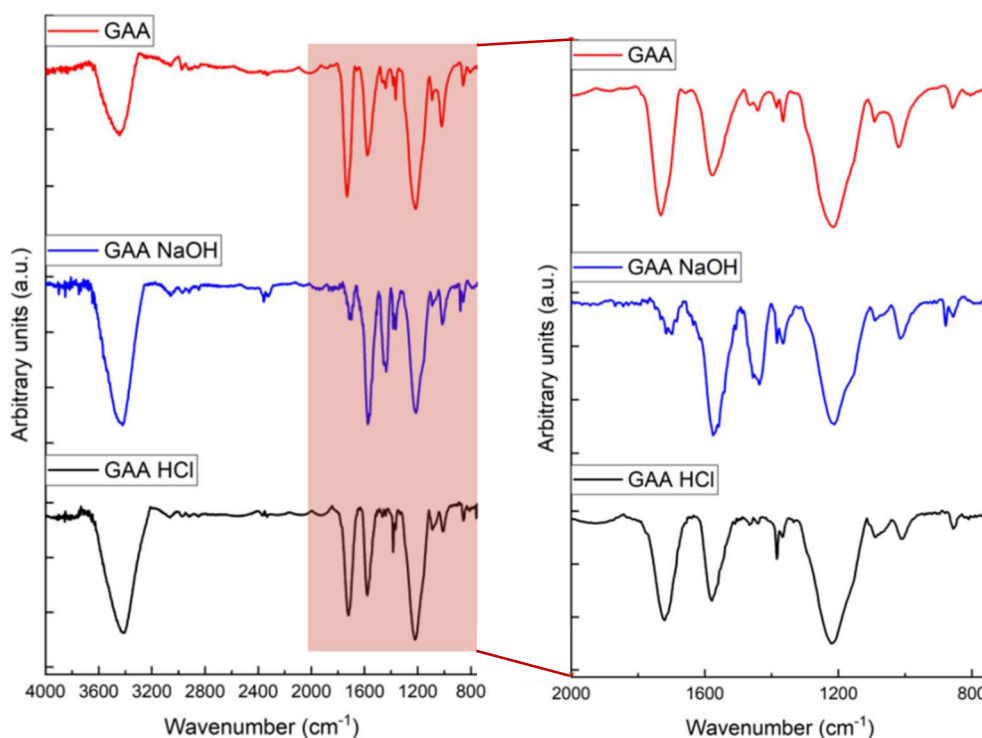


Figure 3.4: Full spectra (left) and zoom (right) of GAA upon basic treatment and subsequent acid treatment.

3.2.4. Solid-state ^{13}C Nuclear Magnetic Resonance

Solid-state ^{13}C -NMR analysis was conducted in collaboration with Prof.s Claudio Garino and Roberto Gobetto from the University of Turin. The non-decoupled spectrum (Fig. 3.5) aligns with the fitting of the C 1s photoemission peak and confirms the presence of 10 at% carboxylic functionalization in the material. In the lower region of the spectrum, two distinct carbon atom peaks can be discerned. The lower peak (5-20 ppm) can be attributed to sp^3 carbon atoms, while the peak at higher chemical shift (30 ppm) arises from the more deshielded carbon atoms influenced by the carboxylic acid. Table 3.2 reports to what extent the carbon atoms present in the material are differently functionalized. The -COOH functionalization degree of 10% further supports the previous data obtained from both XPS and IR analyses.

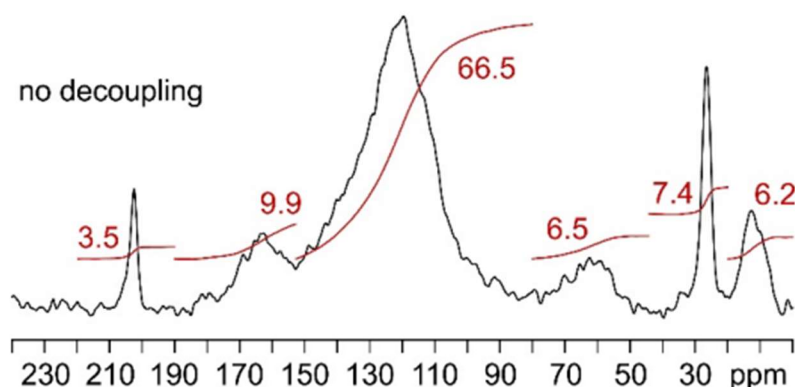


Figure 3.5: GAA Solid state ^{13}C -NMR spectra.

Table 3.2: Peak assignments of the solid state ^{13}C -NMR of GAA.

ppm	Identification	Amount at%
5-20	C (sp^3)	6.2
30	CH_2	7.4
50-70	C-O	6.5
100-150	C (sp^2)	66.5
150-180	COOH	9.9
210	C=O	3.5

3.2.5. Thermogravimetry

Thermogravimetric analysis was conducted by heating the sample at a constant rate up to 800°C under an inert atmosphere, while simultaneously measuring its weight using a microbalance. The results indicate an initial mass loss at 130°C, likely attributed to the desorption of high-boiling-point solvents, most probably water and DMF used during the synthesis (Fig. 3.6). The second and most significant mass loss, accounting for 34.5% of the total material mass, results from the decarboxylation of the carboxylic functionalities. To confirm this, an Evolved Gas Analysis (EGA) should be performed in the future, in order to accurately identify what species are progressively released by the degradation of the material. Since no residual solid was observed at the end of the analysis, we concluded that the prepared GAA does not contain any trace of metals.

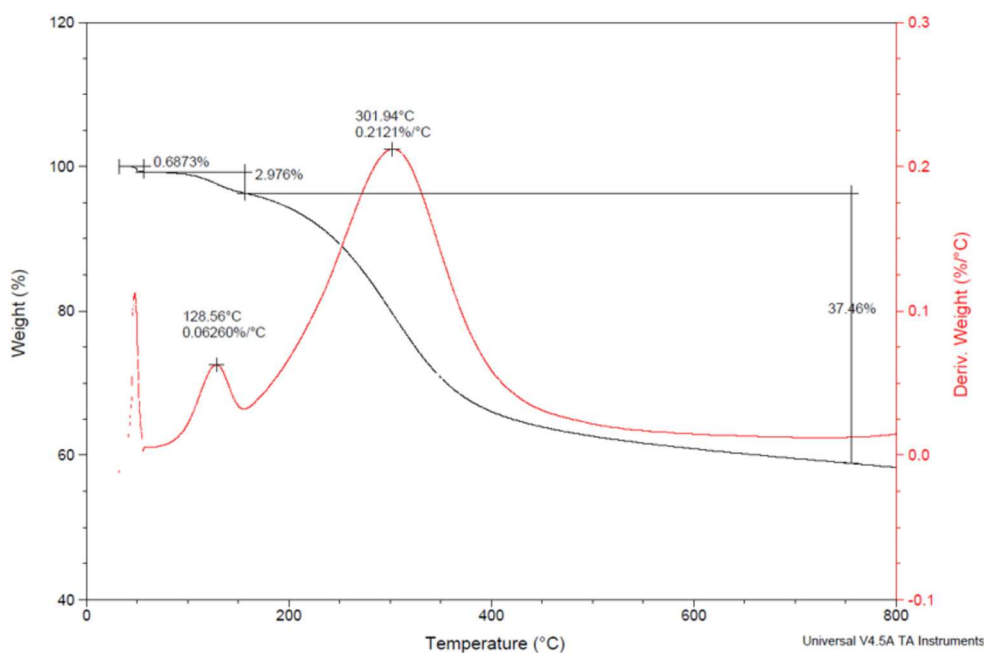


Figure 3.6: Thermogravimetry of GAA.

3.2.6. X-Ray diffraction

X-Ray diffraction was performed on GAA powder, and the obtained diffraction pattern is depicted in Fig. 3.7. The three broad features observed in the pattern can be attributed to the material and resemble those found in graphene oxide [$2\Theta = 11.5^\circ$ (001)] and in reduced graphene oxide [$2\Theta = 24^\circ$ (002) and $2\Theta = 47^\circ$ (102)],⁶⁹ confirming the existence of oxygenated functional groups in GAA. These functional groups lead to an increased interlayer spacing compared to graphite [$2\Theta = 26.5^\circ$ (002)]. The distance between GAA flakes has been calculated by using Bragg's law, resulting in a 0.38 nm gap.

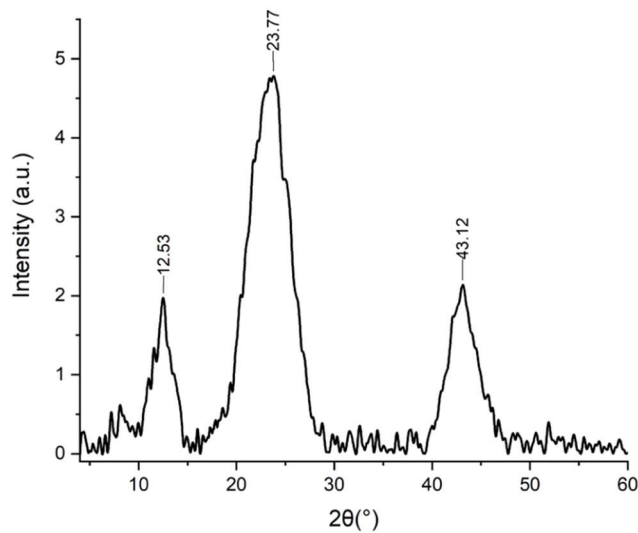


Figure 3.7: X-Ray diffraction pattern of GAA.

3.2.7. Z-potential

Z-potential measurements were conducted to gain insights into the behaviour of GAA in colloidal water suspension. The Z-potential curve at various pH values is presented in Fig. 3.8. Below pH = 5, the potential is approximately zero, indicating a neutral surface charge on the material. Above pH = 5, the Z-potential becomes strongly negative, attributable to the deprotonation of the carboxylic acids.

Beyond its role in determining the surface charge, the Z-potential is particularly useful for describing the stability of the colloidal suspension. In general, suspensions with Z-potential values more positive than +40 mV or more negative than -40 mV are considered stable. This criterion also applies to GAA in the pH range between 5 and 11, implying that the material can be employed in a fairly broad range of acidity conditions.

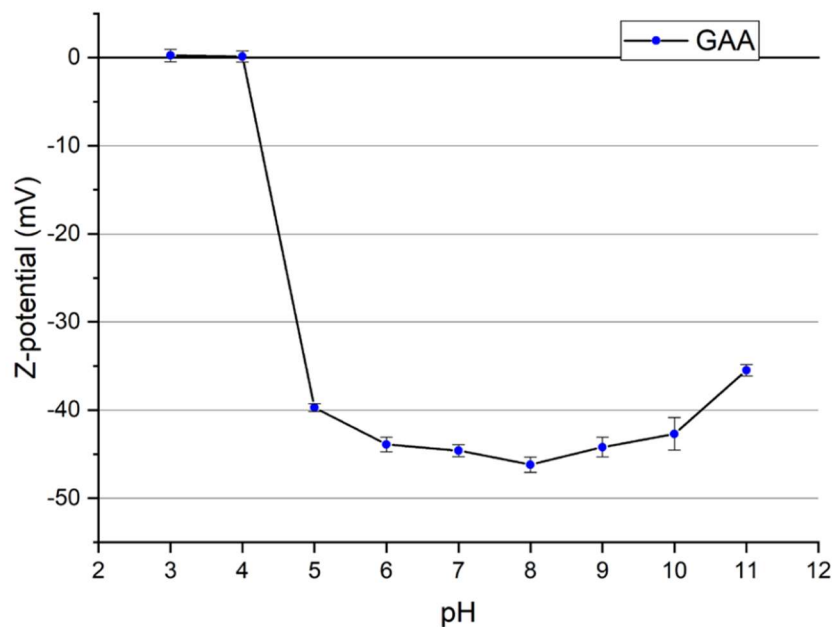


Figure 3.8: Z-potential curve of GAA at different pH values.

3.2.8. Transmission Electron Microscopy

A morphological analysis was conducted through Transmission Electron Microscopy (Fig. 3.9) and compared with those of fluorographene and graphene oxide (Fig. 3.10). In the analyzed sample, the flake dimensions vary from a few nanometers to a few hundred nanometers. Unlike GO and reduced Graphene Oxide (rGO), the nanosheets of graphene acetic acid are smaller, typically by an order of magnitude. These flakes, as expected from a highly functionalized material, are not entirely planar, although exhibiting less wrinkling when compared to fluorographene, primarily due to the presence of sp^2 domains. The edges of the flakes are also wrinkled and kinked, in contrast to graphene oxide and reduced graphene oxide, which is a result of a higher functionalization.

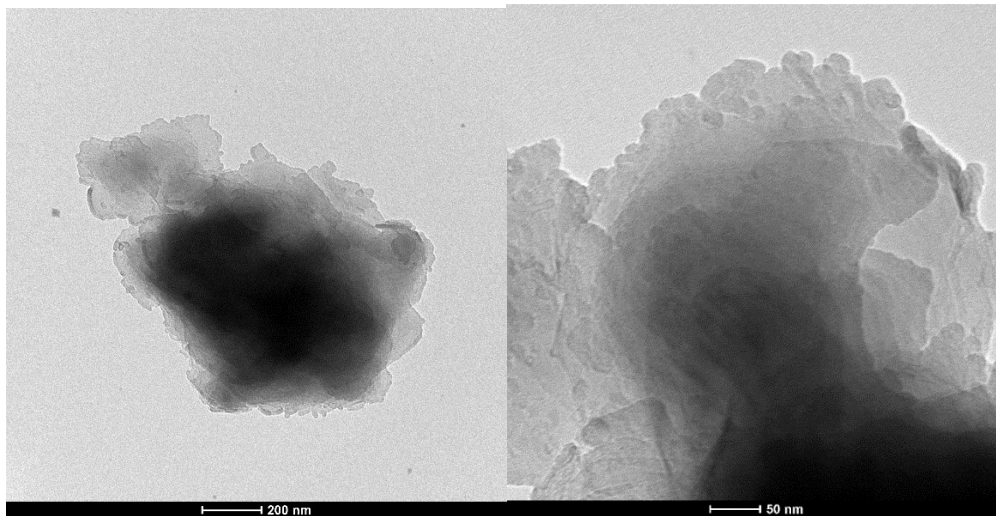


Figure 3.9: GAA TEM image.

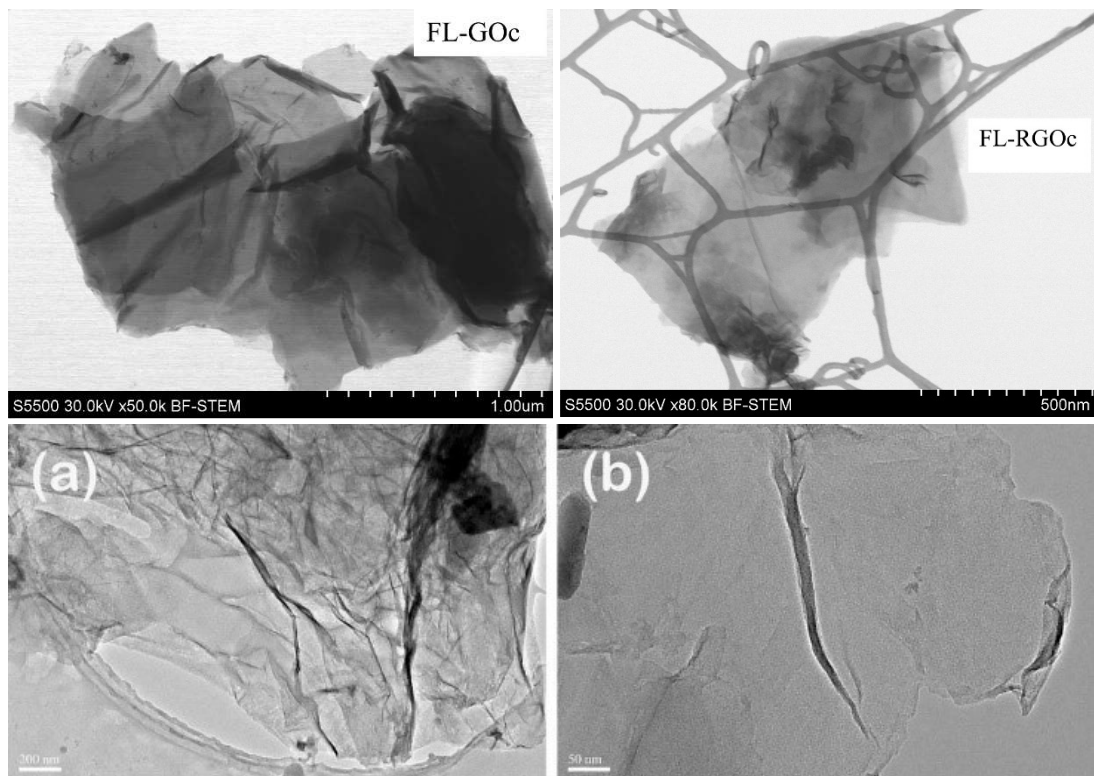


Figure 3.10: GO, rGO (adapted from Stobinski L. et al.⁷⁰) and FG (adapted from Yang Y et al.)⁷¹ TEM images.

Chapter 4

Catalytic tests

4.1. Thioanisole Oxidation

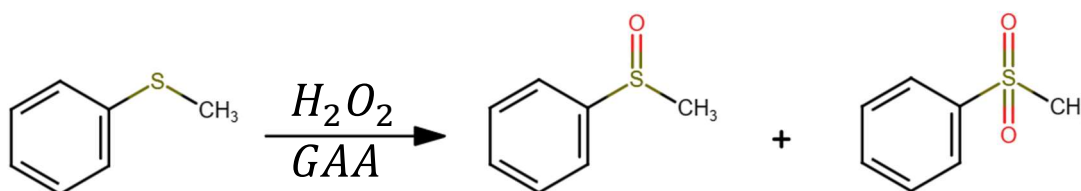


Figure 4.1: Thioanisole oxidation reaction equation.

GAA was evaluated as a carbocatalyst for the oxidation of thioanisole into sulfoxide or sulfone (Fig. 4.1). The study began by adopting the conditions outlined in the work of Abdi and colleagues³⁶ as a reference. We used their methodology as a starting point for our investigation. The progression of the reaction products was monitored through ¹H NMR spectroscopy, with the methyl singlets at 2.51 ppm corresponding to sulphide, at 2.78 ppm to sulfoxide, and at 3.08 ppm to sulfone. Given the utilization of a catalyst similar to that employed by Abdi et al., we anticipated a similar catalytic behaviour and, consequently, similar selectivity towards the sulfones. Another possible catalytic route is that adopted by Bielawski et al., who reached complete conversion of the substrate to sulfoxide with a graphite oxide catalyst, although used in high amount, namely 300wt%.⁷²

The reaction was carried out under neat conditions, specifically in complete absence of solvent, in a Teflon-capped vial. The reaction mixture was prepared by dispersing

20 mg of GAA in 0.3 mL of H₂O₂, resulting in a black slurry. Subsequently, 0.117 mL of thioanisole were added, and the mixture was left to react for 2 hours at 25°C.

After the allowed reaction time, an NMR spectrum was collected. With the first few experiments, nearly complete conversion from thioanisole to sulfoxide was always observed, even for shorter reaction time. Following Abdi et al. procedure, 1 mL of ethanol was used to extract the product through centrifugation and subsequent rotary evaporation of the supernatant. We later found out that such separation process caused the evaporation also of the residual unreacted thioanisole, due to its low surface tension of 0.7±0.3 mmHg at 25°C, thus greatly overestimating the reaction conversion. To circumvent this issue, instead of trying to isolate the reaction products, the conversion was determined via NMR analysis of the crude reaction mixture (Fig. 4.2). To enable this, it was necessary to change the solvent, since ethanol exhibited a broad feature around ranging from 3 to 4 ppm that prevented an accurate conversion determination for the reaction. A suitable solvent was then required that could dissolve both the thioanisole and hydrogen peroxide, while not displaying signals at the NMR analysis that could interfere with the ones arising from the product. After conducting several tests, tetrahydrofuran was identified as the most suitable solvent for this purpose.

With the use of THF it was possible to calculate the yield of the reaction with Eq. 1, where $A_{sulfide}$, $A_{sulfoxide}$, and $A_{sulfone}$ are the integrated area of the methyl group NMR peak, which is found at 2.51 ppm, 2.78 ppm and 3.08 ppm for the sulfide, the sulfoxide and the sulfone, respectively.

$$Yield = \frac{A_{sulfoxide}}{A_{sulfide} + A_{sulfoxide} + A_{sulfone}} \quad \text{Eq. 1}$$

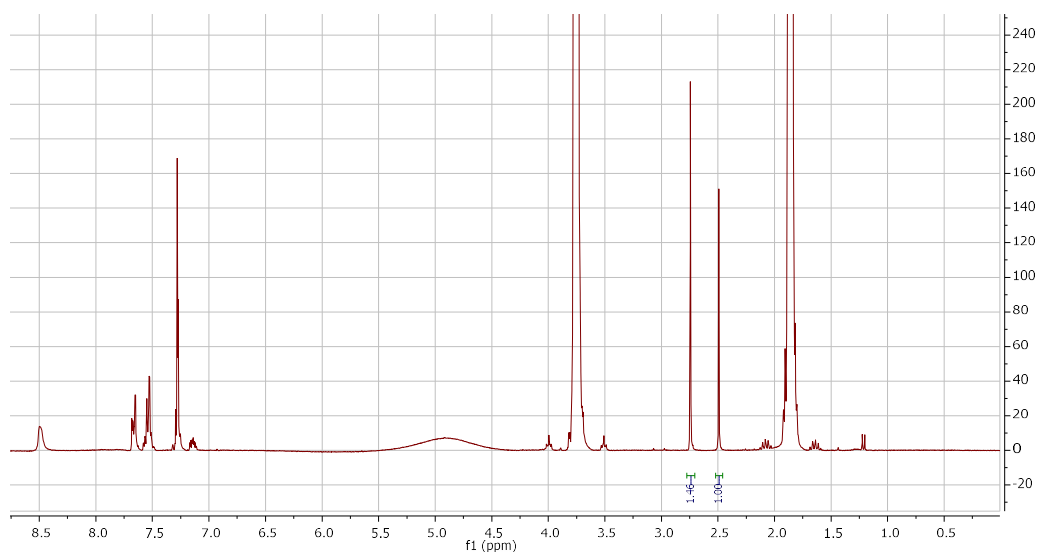


Figure 4.2: ^1H NMR spectrum of reaction crude in CDCl_3 obtained using 20 mg of GAA after 1 hour.

With this new setup, we collected the first kinetic curve, which revealed complete conversion to sulfoxide in approximately 130 minutes (Fig. 4.3), similarly to Bielawski et al. work, but at the use of far less material, namely a concentration of 1 wt% instead of the 300 wt% reported in their work and at much lower temperature (room temperature in the present case vs 100°C).

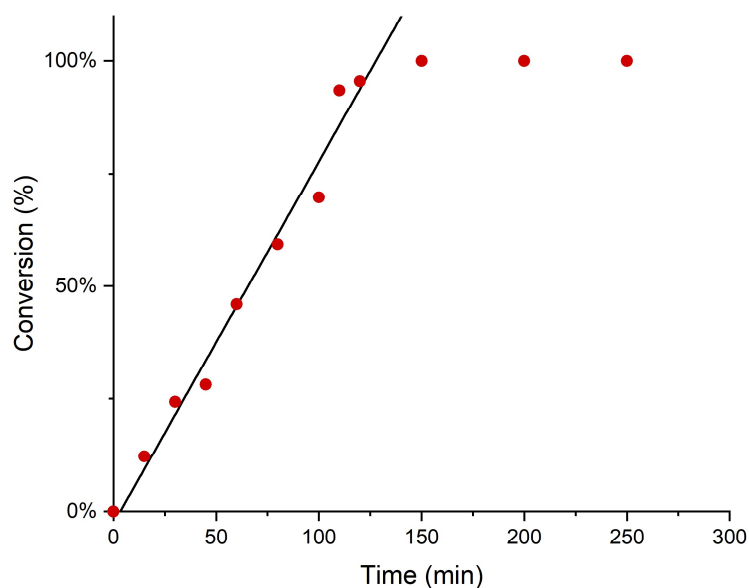


Figure 4.3: Kinetics of thionisole oxidation using 20 mg of GAA as a catalyst.

This finding is intriguing as the material proposed by Abdi et al., which was closer to GAA than the one used by Bielawski et al., exhibited the opposite behaviour, demonstrating strong selectivity towards sulfone formation. Such discrepancy may be attributed to the distinct distribution of functionalities in the two materials. In the case of GAA, most of its acid functions are dispersed across the material's surface, resulting in a lower local function density. In contrast, the material synthesized by Abdi et al. possessed a higher local function density on the edges, which implied the presence of adjacent acid functions. Therefore, the mechanism they proposed involved a double oxidation of the thioether substrate catalysed by two adjacent acid functions, leading to sulfone formation.

Such difference in the functionalization distribution can be ascribed to the different synthetic path adopted in this thesis with respect to the mentioned work. By using fluorographite as the starting substrate, in fact, the functionalization of GAA results more evenly distributed over the material's whole surface, and not localized only on the edge of the sheets. This outcome was expected based on previous results obtained for the graphene acid reported by Otyepka³³ et al., which share a very similar synthetic route.

Consequently, it is less likely to have two acid functions in close proximity over the surface of the GAA sheets, and so to have the simultaneous double oxidation of the thioether through the mechanism proposed by Abdi et al.

To confirm the selectivity towards sulfoxide, a 24-hour catalytic test was conducted, in which no sulfone formation was observed. It is worth noting that the selectivity observed with GAA aligns with the findings of Golchoubian and Hosseinpoor in their oxidation of various sulfides using hydrogen peroxide and acetic acid.⁵⁷ Hence, we can

assume that the acetic acid functionalization plays a predominant role in the oxidation of thioanisole.

Regarding the hydrogen peroxide activation mechanism, we hypothesize that the material acts in a similar manner to the AGO reported by Abdi et al.³⁶ This material interacts with H₂O₂ through its acid functionalities forming hydroperoxide, which serves as a potent oxidizing group. Due to the high reactivity of hydroperoxides and the intrinsic difficulty in their analysis, it was not possible to confirm such hypothesis during the thesis, so future studies will need to address this specific aspect as well.

The substantially lower conversion observed under solvent-free conditions for GAA with respect to AGO can be attributed to the lower amphiphilic nature of the former. In fact, both AGO and GAA possess a hydrophobic basal plane and hydrophilic functional groups (-COOH), but they differ for the distribution of such groups across the material. As described before, GAA presents carboxylic moieties over the whole sheets, which enhances the hydrophilic properties with respect to the hydrophobic ones. This consideration may explain the lower activity displayed by GAA when compared to AGO, which in the same conditions and using the same mass ratio reached almost complete conversion in around 60 minutes, in contrast with the 130 minutes necessary to reach the same conversion for GAA. In fact, the stronger interactions between GAA and water, which is a non-solvent for thioanisole, reduces those with the substrate.

Nevertheless, it should be considered that beside the lower activity, by comparing the turn-over frequency of both materials, GAA outclasses AGO by over two orders of magnitude, indicating a more effective use of the single catalytic center.

Furthermore, Otyepka discovered that carboxylic functionalities on the surface of the material tend to form interlayer hydrogen bonds. This finding could explain the lower

reaction rate observed when using GAA in solvent-free conditions, because the absence of other chemicals species to bond with may have led to stronger interactions between the material's layers. It also should be noted that the acetic acid moieties present in our material are generally more mobile than those of AGO, due to an additional $-CH_2-$ unit. More configurations becoming available to form hydrogen bonds would lead to more favored and stronger interactions. This constitutes a further obstacle for the coordination of the substrate to the catalyst surface, since the associated energy barrier would further increase. On the other hand, the absence of a reaction solvent, apart for the water of the hydrogen peroxide 30% solution, is a major advantage that could be exploited in industrial applications to lower waste production.⁷³

What's more interesting is the observed linear trend in the kinetics. We attributed this linearity to an excess of catalyst with respect to the reagent. To further investigate this aspect, additional analyses were performed by reducing the total catalyst amount from 20 mg to 1 mg (Fig. 4.4).

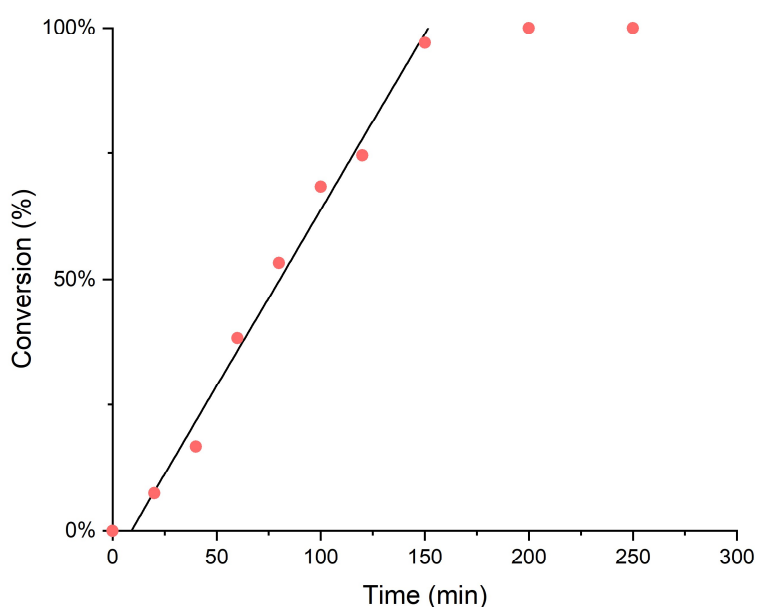


Figure 4.4: Kinetics of thioanisole oxidation using 1 mg of GAA as a catalyst.

A linear trend was observed again, though this time a slight reduction in its slope was observed, from 0.80 to 0.70. This outcome led us to suspect that the catalyst was still present in excess. To assess the material's properties more rigorously, a single experiment was conducted with only 0.1 mg of catalyst, and the results were compared with the activity of uncatalyzed hydrogen peroxide (Fig. 4.5). Remarkably, even with such a small quantity of material, the conversion increased to 35%, from the 15% achieved with hydrogen peroxide alone.

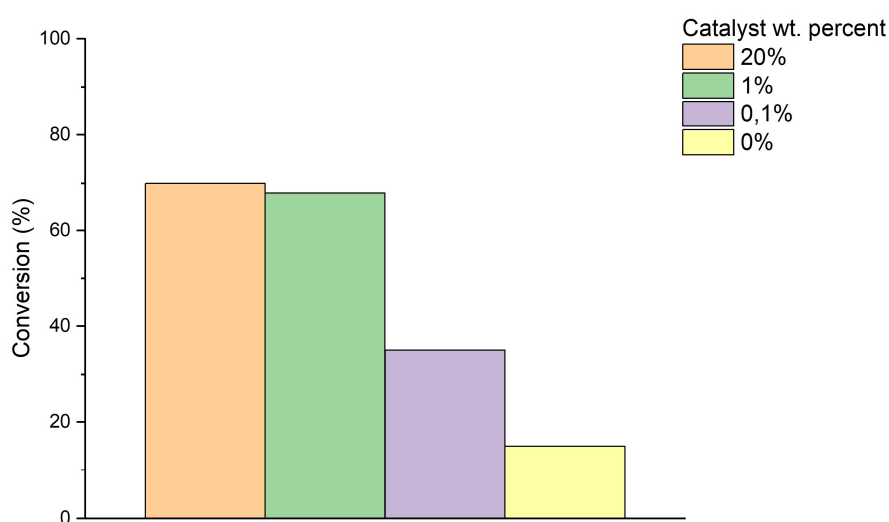


Figure 4.5: Comparison between percent conversions achieved after 100 minutes of reaction varying GAA concentration.

It is worth noting that in 2011 Bielawski used “graphite oxide” (defined as “graphene oxide” by modern nomenclature) to catalyse the oxidation of thioether to sulfoxide.⁷² Doubts on the actual ability to catalyse the reaction have however been posed and further investigated by Presolski and Pumera.³⁹ They tested the material as a catalyst for the benzyl alcohol oxidation reaction and found it to be more of a stoichiometric reagent than an effective catalyst.

Being GAA a graphene-based material bearing high quantities of oxidized groups as GO, we considered the hypothesis that it acted as well as a stoichiometric oxidant instead as a proper catalyst, speeding up the reaction but being depleted at the same

time. Hence, several tests were conducted to confirm that the material functioned as an effective catalyst. In the first test, hydrogen peroxide was substituted with pure water, but no reaction occurred.

In a second experiment, using 1 equivalent of hydrogen peroxide, the conversion was observed to drop by 40% with respect to the one reached during the tests with 3 equivalents of H_2O_2 . This was an expected outcome, because the optimal thioether/hydrogen peroxide ratio to obtain the maximum reaction yield using the lowest amount of oxidant, has been established to be 1:2.⁷⁴

GAA had been previously tested by the research group for the thermal activation of oxygen to catalyse the oxidative homocoupling of amines, reaching a conversion of 86% in 6 hours. Based on such results, it was supposed that in the studied thioether oxidation, the real oxidant was atmospheric oxygen rather than hydrogen peroxide. This hypothesis was verified by performing the reaction at 60°C in an open-air environment without the use of H_2O_2 , but no conversion was detected, proving that atmospheric oxygen does not participate in the catalytic process. Another test was performed with hydrogen peroxide in an inert nitrogen atmosphere, yielding similar activity to the aerobic conditions and further confirming the previous conclusions.

The above reported tests have confirmed the capacity of GAA to oxidize thioanisole but have not discerned between the possibility of a catalytic hydrogen peroxide activation and the one of a stoichiometric oxidative reaction. Besides the amount of oxygen necessary to completely oxidize thioanisole is not contained in the material, recycling test were conducted to assess that the material was indeed exhibiting catalytic activity and not undergoing reduction during the reaction.

This involved washing the recovered GAA with acetone and water, followed by its reuse in subsequent runs. Remarkably, the results demonstrated no loss in activity or

alteration in selectivity even after 8 cycles (Fig. 4.6). Additionally, XPS data collected on the material recovered after these 8 recycling cycles confirmed that no change in composition had occurred, and that the material still presented the original amount of carboxylic functions, hence retaining its original catalytic activity.

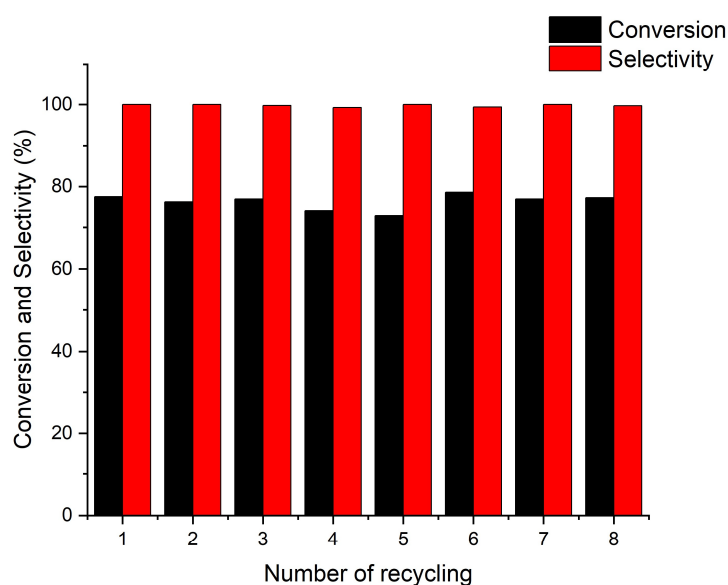
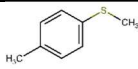
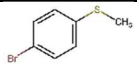
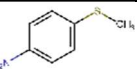
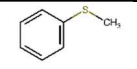
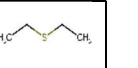


Figure 4.6: Conversion and selectivity of GAA across subsequent recycling cycle.

Given the appealing performance and the unusual selectivity of the catalyst, we expanded the scope of the reaction. Keeping fixed all the system variables (temperature, composition, reaction time, etc...), various thioanisole derivatives bearing different substituents and diethyl sulfide were selected to investigate the reaction mechanism (Table 4.1). As expected for an oxidation reaction, the presence of activating groups such as hydroxyl and amino groups significantly accelerated the reaction, thanks to their electron donating properties. Conversely, deactivating groups such as bromine slowed down the reaction. What's particularly compelling is the behavior of methyl thioanisole which, despite bearing an activating group, exhibited a slight deceleration of the reaction. Possible explanations for this phenomenon could be the larger steric hindrance of the substrate, or its less hydrophilic character, both factors that could reduce the strength of the interactions with the catalyst surface.

It is not surprising that the only alkyl thioether included in the scope of the reaction showed a higher conversion, because of its increased reactivity compared to benzyl thioethers. On the other hand, it is interesting to note how the reaction with methyl thioaniline yielded results comparable to the one with diethyl sulfide, thus showing how a strongly activating group like $-NH_2$ can increase the reactivity of benzylic thioethers up to that of alkyl ones. Notably, the amino group did not undergo oxidation during the reaction. In the future, XPS analyses could be performed on GAA after the reaction with methyl thioaniline with the aim to verify that neither reagent nor product poison the catalyst by forming permanent amidic bonds with the material.

Table 4.1: Conversion and selectivity of GAA in the oxidation of different thioether substrates.

						
Conversion (%)	65	59	44	98	99	99
Selectivity toward sulfoxide (%)	100	98	100	100	93	96

By comparing the results of this study with the latest publications regarding the catalytic thioanisole oxidation (Table 4.2), it can be seen how GAA covers a deficiency of conventional metal catalysis. In fact, although most metal catalysts present higher conversion rates than GAA, they lack in selectivity: none of the examined metal-based catalysts selectively converts the substrate into one single product. The highest reported selectivity among the metal-based options is 70%, and was achieved by Xie et al. by using a 8-quinolinato Mn(III) complex, in stark contrast with the 99% herein obtained with GAA.

Examining next other metal free catalysts, direct comparison with AGO underlines how the two materials present comparable conversion rates, but opposite selectivity, being potentially complementary to each other. Another possibility for the metal free

catalysis of the reaction is using non-carbonaceous materials, like organic dyes capable to photo activate oxygen as the ones proposed by Wenliang Li et al.⁷⁵ The major advantage consists in the utilization of an abundant and green oxidant as oxygen, whose activation is not trivial, but the long-time reaction and the employment of an highly energy consuming light source during the whole process are two major drawbacks that could hinder the industrial implementation of such technology.

Regarding the turn-over frequency (TOF), we find that vanadium oxide presents the highest value among all considered options. Nonetheless, GAA performance is in line with that of other metal-based catalysts, if not slightly better. Sensible TOF improvement is instead assessed with respect to AGO.

It is necessary to take into account that the TOF of the different catalysts was evaluated at the completion of the reaction due to lack of reported data, and the comparison may not be entirely reliable. However, since the determination of the exact amount of the catalytic centers present on the several catalysts is not trivial, the TOF was the only figure of merit available for a sensible comparison.

Table 4.2: Reaction conditions and performance parameters for the thioanisole oxidation reaction with different catalysts. TOF has been calculated at reaction completion.

	Catalyst concentration	Oxidant	Time (min)	Temperature (°C)	Solvent	Conversion (%)	Selectivity (%)	TOF (s ⁻¹)
GAA	1 wt%	H ₂ O ₂ 1:3	150	RT	none	99	99	0.02
AGO ³⁶	20 wt%	H ₂ O ₂ 1:3	60	RT	none	95	10	0.0001
Mn(III) complex ⁵⁵	0.2 mol%	H ₂ O ₂ 1:2	120	RT	H ₂ O/ac etone 1:3	93	71	-
Organic Dyes ⁷⁵	0.5 mol%	air	24 hours	RT	CH ₃ OH	99	99	-
Anchored Oxovanadium ⁷⁶	0.8 mol%	H ₂ O ₂ 1:2	20	RT	CH ₃ CN	99	70	0.064
SrTiO₃ ⁷⁴	10 wt%	H ₂ O ₂ 1:2	60	50	CH ₃ CN	40	53.8	0.0018
SrTiO₃/Nb₂O₅ ⁷⁴	10 wt%	H ₂ O ₂ 1:2	60	50	CH ₃ CN	92.5	30	0.01

4.2. Hydrogen peroxide disproportionation

It was previously reported how GAA can activate hydrogen peroxide. In a prior work not included in this thesis, Agnoli's group discovered its exceptional peroxidase-like activity. Taking this into account, we conducted experiments to ascertain if GAA could catalyse the disproportionation of hydrogen peroxide (Fig. 4.7) in a manner similar to catalase enzymes.

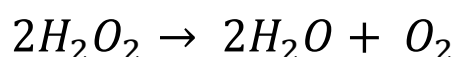


Figure 4.7: Hydrogen peroxide disproportionation reaction equation.

Our initial approach to assess the reaction's activity involved using Ti(IV) oxosulfate. This forms a complex with hydrogen peroxide, characterized by its distinct yellow colour and strong UV-Vis absorption, making it suitable for hydrogen peroxide determination in solution. To achieve this, we established a calibration curve in collaboration with Prof. Centomo.

To employ such technique effectively, the solution's pH must not exceed 2.5 because the titanium complex breaks down and forms insoluble titanium dioxide, leading to scattering phenomena. To prevent this, the hydrogen peroxide solution was acidified before adding the complex.

Another issue affecting hydrogen peroxide determination was scattering caused by the presence of materials remaining from the separation process. We explored centrifugation and filtration, but in both cases some nanoparticles persisted. In fact, transmission electron microscopy (TEM) revealed the presence of nanoparticles with size under 200 nm, smaller than the filter's pore size (0.2 μm) used for the separation. To assess the impact of these scattering phenomena, we collected different calibration curves (Fig. 4.8): the first was generated using only water, the second with unseparated material, and the last after filtration and centrifugation. These three curves exhibited

different slopes and were unsuitable for determining hydrogen peroxide levels. Moreover, mathematical correction after analysis is not feasible due to the unpredictable nature of the scattering effects.

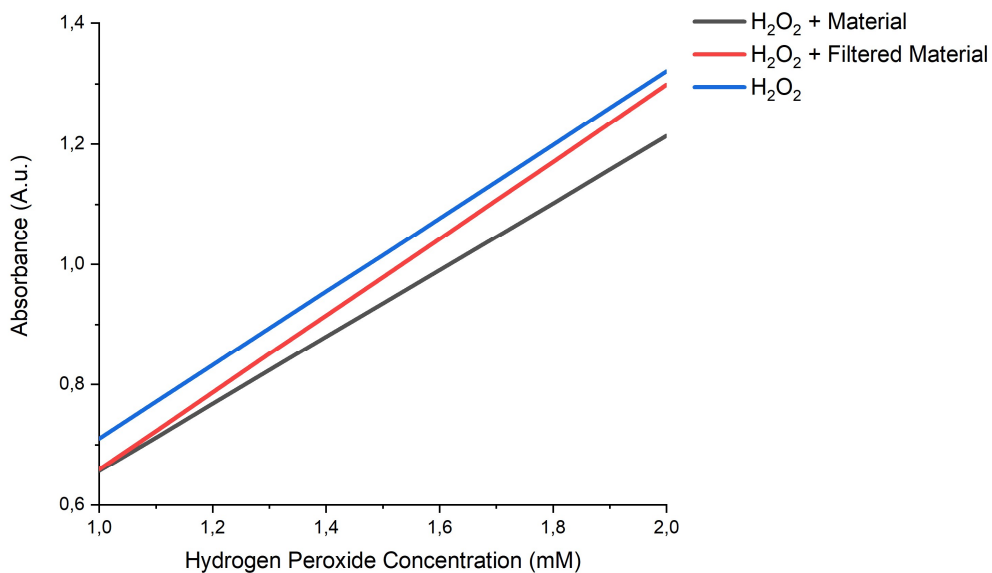


Figure 4.8: Ti(IV) oxosulfate calibration curves.

Another method to determine the amount of disproportionated hydrogen peroxide is to measure the quantity of oxygen produced. For this purpose, we employed a specific oxygen probe (Fig. 4.9) provided to us by Prof. Sartorel. This probe is based on a unique metal complex, the excited state lifetime of which depends on the quantity of oxygen in the surrounding atmosphere. The specific stoichiometry of such complex is property of Ocean Insight and its physical properties were not reported, making it unsuitable for direct calculation. To ascertain the oxygen concentration, we performed a calibration by introducing known quantities of pure oxygen (Fig. 4.10).



Figura 4.9: Neofox Oxygen probe developed by Ocean Insight.

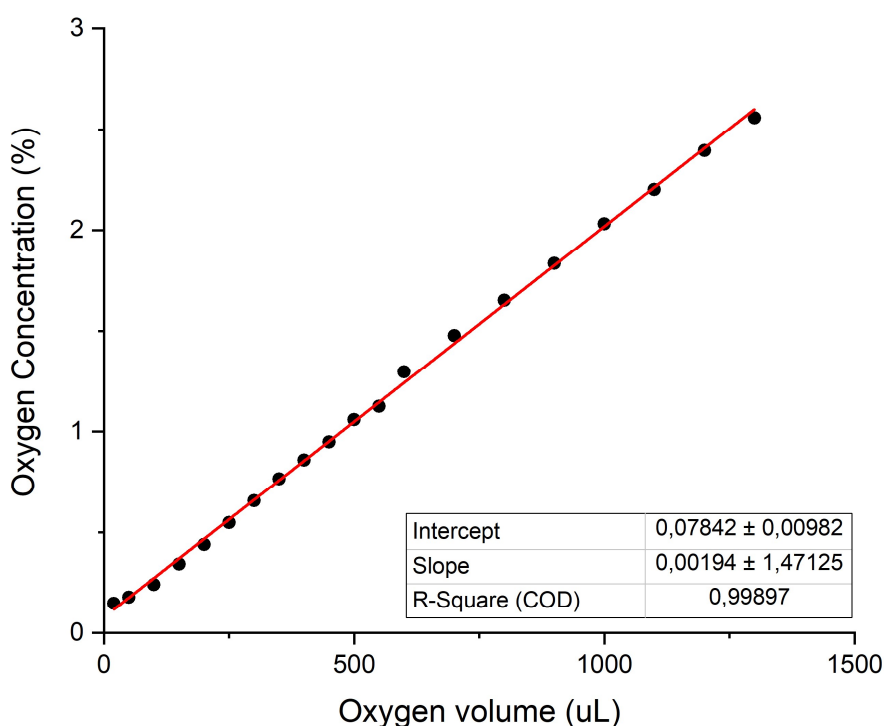


Figure 4.10: Oxygen probe calibration curve.

The experimental setup is depicted in Fig. 4.11. The reaction is carried out in a three-necked round-bottom flask, each neck sealed with a rubber stopper. The necks are equipped with connections for a nitrogen line, the oxygen probe, and a vent for overpressure release. Material dispersion and the hydrogen peroxide solution are introduced using a syringe once an inert atmosphere is achieved.

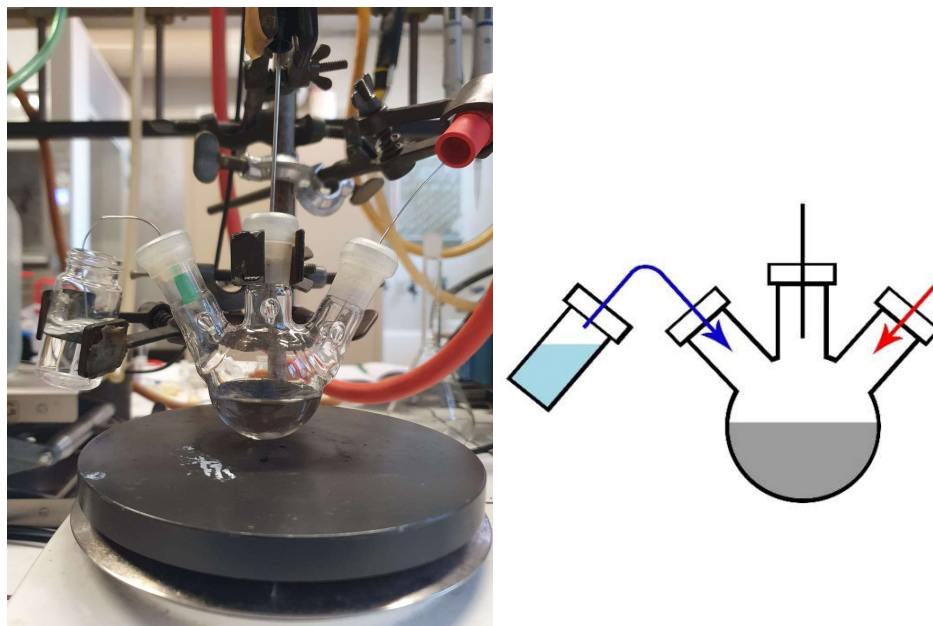


Figure 4.11: Experimental setup used for catalytic tests in the disproportionation of H_2O_2 .

With the optimized setup and the calibration curve, it was possible to investigate the catalytic behaviour of GAA (Fig. 4.12). We tested 10 mL of a 0.16 M hydrogen peroxide solution with a catalytic amount equivalent to 1 wt%, yielding poor results. After ten minutes, only 0.75% of the total hydrogen peroxide had degraded. Furthermore, the initial increasing trend quickly reached a plateau. We experimented with both higher and lower concentrations, but no significant improvements were observed. The concentration that yielded the best results was 2.7 wt%, although it still fell short of achieving the expected hydrogen peroxide disproportionation. It's worth noting that all tests were conducted for one hour, even though not all results have been reported, and most of them reached a plateau in around 20 minutes.

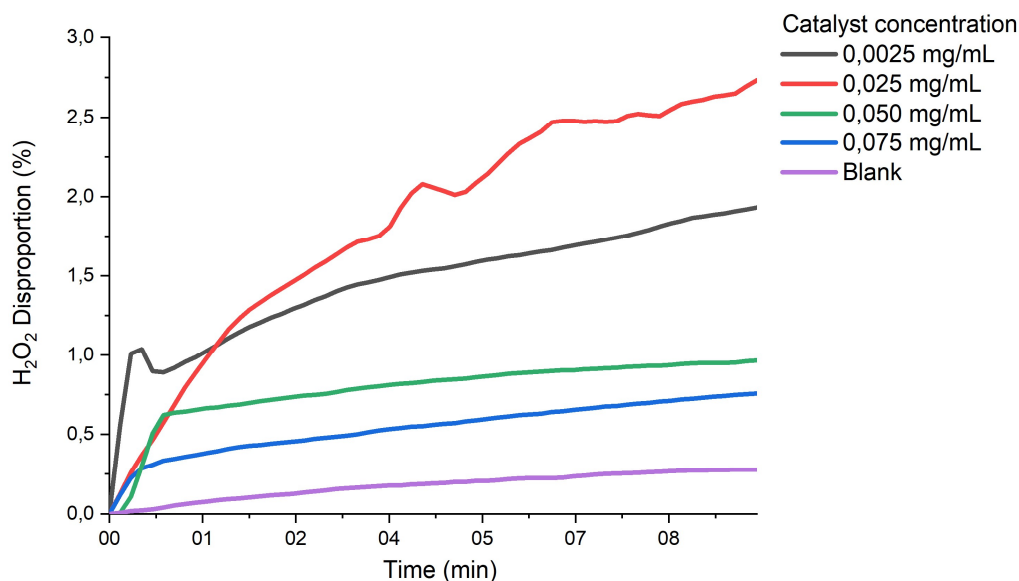


Figure 4.12: Hydrogen peroxide disproportionation at different catalyst concentrations.

We increased the hydrogen peroxide concentration to confirm the material's inactivity. To achieve this, we selected a material concentration that yielded better results. It was observed that the lower the hydrogen peroxide concentration, the greater the disproportionation (Fig. 4.13).

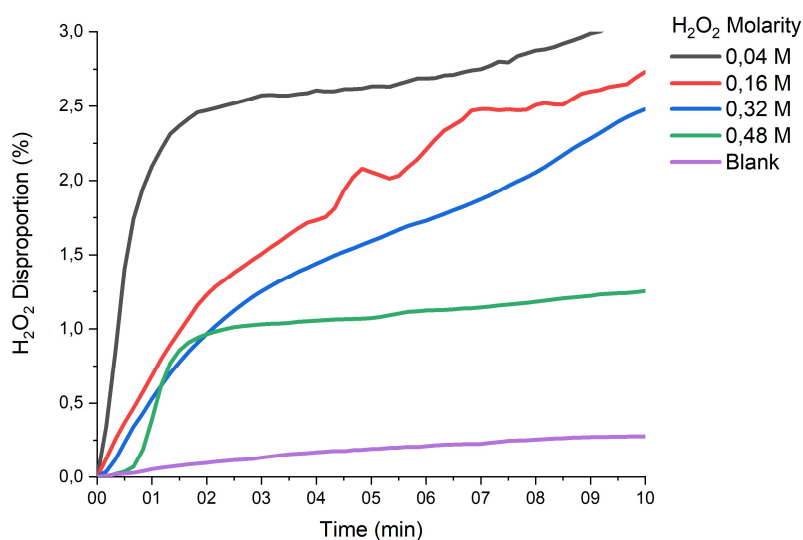


Figure 4.13: Hydrogen peroxide disproportionation at different H_2O_2 concentrations.

The limited extent of hydrogen peroxide disproportionation and the rapid deactivation of the material led us to conclude that GAA may not be a suitable candidate for catalase mimicking. This result was unexpected, considering GAA's efficacy as a catalyst for oxidative reactions. Moreover, previous experiments confirmed its interaction with

hydrogen peroxide. It is probable that the formation of hydroperoxyl acid on the material, without the presence of a sacrificial species, prevents further reactions, resulting in low hydrogen peroxide utilization. The observed maximum trend in material concentration, in contrast to this finding, could be attributed to aggregation phenomena. In fact, magnetic stirring alone is insufficient to maintain the material in a well-dispersed state.

Chapter 5

Conclusions

During this project we developed a synthetic route to synthesize graphene acetic acid (GAA), a novel graphene derivative bearing carboxylic functionalities. We started from fluorographite, a cost-effective and largely used material available in large quantities. Furthermore, it has been proved that stoichiometric C_1F_1 materials like fluorographite could be synthesized by recycling fluorinated polymers, reducing the quantity of fluorine waste. By using non-toxic, sustainable reagents and environmentally friendly solvents we were able to obtain large quantities of GAA, with reproducible properties between synthetic batches. In addition, the process is carried out at low temperatures and at ambient pressure, both excellent prerequisites for a green scalable synthesis. The structural and chemical properties of GAA were characterized by various techniques to assess the presence of the sp^2 domains typical of graphene-based materials, as well as the nature and degree of the functionalities. In particular, XPS analysis revealed a high functionalization degree around 10% of the total carbon atoms, and the absence of residual fluorine in the material.

We have investigated the catalytic behaviour of GAA by first testing an important prototypical reaction as the oxidation of thioethers to sulfoxides and sulfones using hydrogen peroxide as oxidant. We discovered that not only the reaction was speeded up by the presence of GAA, but also that the selectivity was reversed with respect to

the one exhibited by the benchmark material AGO, resulting in the preferential formation of sulfoxides. That was unexpected, due to the similarity between the functionalities present in GAA and in AGO.

The catalyst was further studied through a scope of the reaction, in which we discovered that the oxidation was even more favourable for benzyl thioether substrates bearing strongly activating groups. In the end, a sequence of recycling tests has been performed to assess the actual catalytic behaviour of the material. The overall performance of GAA was then compared with most of the recently published metal-based catalysts, finding out that it surpassed them in terms of selectivity, with the major advantage of no metals required. We also tested the ability of the material to catalyse the disproportionation of hydrogen peroxide. Unfortunately, the material revealed to be inactive as a catalyst. In particular, it has been supposed that the lack of a sacrificial species to be oxidized could inhibit the interaction of hydrogen peroxide with the material.

Future studies on GAA could address several potential applications besides those already explored within this work. The ability of the material to activate hydrogen peroxide can be exploited for the oxidation of several organic substrates, for example in the treatment of wastewaters. In the research group, GAA was previously tested also for the activation of atmospheric oxygen, in view of its potential application for the synthesis of hydrogen peroxide. If properly explored, such possibility could solve the necessity to introduce hydrogen peroxide as a ready-made chemical for the reactions listed before: generating it in situ from a greener source as oxygen could make the whole process more sustainable.

Another possibility is the further functionalization of the carboxylic acid groups. Amidic and ester bonds have already been tested by the group and in both cases high

yields of the desired graphene derivative have been obtained. Such materials open new ways for the chemistry of GAA, where the first would be able to strongly bond other substrates, while the second could enable reversible bonds, which constitute a promising property for designing advanced drug delivery systems. The non-toxicity of the material would have to be assessed by in vivo tests. Other alternative functionalizations could be explored for the heterogenization of other catalysts, which would require in depth studies on GAA stability under such catalysts' typical working conditions. Besides the high functionalization degree, graphene acetic acid retains all the interesting electrical proprieties of a graphene-based material, which could be exploited in applications involving linked photoactive molecules and chromophores. Regarding this potential application, with the help of Prof. Casalini GAA has recently been used for the development of a liquid gated transistor and a supercapacitor, underling its outstanding electrical proprieties.

The research group is also currently testing the implementation of GAA inside microfluidic reactors. One of the major advantages of microfluidics is the fine control over the reaction conditions. Being GAA an heterogenous nano dimensional material, a microfluidic reactor could be designed with GAA-decorated microtube inner walls. Since one of the industrial sectors taking the most advantage of microfluidics is the pharmaceutical industry, GAA could be a promising option to reduce reaction times and operate in milder conditions for the production of fine chemicals over a larger scale. Such proposal is particularly supported by the fact that more than 30% of US-FDA approved drug contain sulfur, some of which specifically as sulfoxide.⁷⁷

Chapter 6

Experimental section

6.1. Synthesis of GAA

In a 250 mL three-necked round-bottom flask, 333 mg of fluorinated graphite (FG) were suspended in 50 mL of N,N-dimethylformamide (DMF) that had been previously dehydrated through a vacuum-nitrogen cycle. The material was exfoliated via ultrasonication for 4 hours at room temperature, and the suspension gradually changed from milky white to light brown. Concurrently, a mixture of 26.6 g of calcium carbonate, 13.3 mL of diethyl malonate, and 50 mL of DMF was stirred for at least 1 hour in an ice bath at 0°C. After the sonication of FG, the diethyl malonate mixture was added to the round-bottom flask, and they were heated to 130°C for 24 hours under magnetic stirring. By the following day, the mixture had turned black.

After the mixture naturally cooled down to room temperature, it was vacuum-filtered over a polytetrafluoroethylene membrane (PTFE, 0.2 µm pore size). The black powder obtained was then washed with acetone (3x100 mL) and removed from the filter. Another cleaning filtration on a polycarbonate membrane was performed to remove the remaining potassium carbonate and other insoluble salts in organic solvents.

The recovered black powder was dispersed in 100 mL of Milli-Q water in a 250 mL round-bottom flask and sonicated for 4 hours at room temperature. Then, a few drops of 98% sulfuric acid were added to the flask until the pH of the mixture reached 1-2.

The flask was placed under reflux at 100°C overnight, and the solute was then recovered through vacuum filtration over a polycarbonate membrane (PC, 0.2 µm pore size). The material was cleaned with (3x100 mL) of Milli-Q water, then dispersed in the least amount of ethanol and dried via rotary evaporation. Through this process, we consistently obtained around 200 mg of pure GAA.

6.2. Base and acid treatment of GAA

10 mg of GAA were suspended in 10 mL of a 1M NaOH solution and sonicated for 1 hour at room temperature. The material was then filtered (without washing) using a PC membrane to obtain GAA-NaOH. Subsequently, this was suspended in 10 mL of a 1M HCl solution and sonicated for 1 hour at room temperature. It was then filtered (without washing) using a PC membrane to obtain GAA-HCl.

6.3. Physicochemical characterizations

The surface chemical characterization of the material has been carried out using X-ray photoelectron spectroscopy (XPS) in a custom-made UHV system working at a base pressure of 10^{-9} mbar, equipped with an Omicron EA125 electron analyzer and an Omicron DAR 400 X-ray source with a dual Al-Mg anode. Core level photoemission spectra (C 1s, N 1s, O 1s, F 1s) were collected at room temperature with a non-monochromated Al K α X-ray source (1486.7 eV) and using an energy step of 0.1 eV, 0.5 s of integration time, and 20 eV of pass energy. The samples were suspended in 2-propanol and drop casted on a Cu sample holder. Solid state Fourier Transformed Infrared (FT-IR) spectra were recorded on a JASCO FT/IR-4100 spectrometer by dispersing the material in KBr. Transmission Electron Microscopy images were acquired using a FEI Tecnai 12 transmission electron microscope. XRD 46

measurement were acquired using a Bruker D8 Advance instrument with a Cu K α XRay source (0.15406 nm) at 40 kV and 40 mA. Z-potential measurements were acquired on Malvern Panalytical Zetasizer Nano ZS90 instrument using 0.3 mg/mL suspensions of GAA in water. The pH was tuned between 3 and 11 using NaOH, HCl and NaCl to maintain constant ionic strength. ¹H NMR spectra were acquired in CDCl₃ using a Bruker Avance spectrometer operating at 300 MHz and analyzed with the Topspin software. We gratefully acknowledge Professors Claudio Garino and Roberto Gobetto from University of Turin for their work on the solid state ¹³C NMR spectroscopy. The thermal elemental analysis was conducted using FLASH 2000 CHNS analyzer with the help of Dott. Loris Calore.

6.4. Thioether oxidation

In a 25 mL round-bottom flask, the required amount of graphene acetic acid (GAA) was added for the experiment. It was then dispersed with 0.3 mL of 30% hydrogen peroxide (H₂O₂) and sonicated for 10 minutes at room temperature. Subsequently, 1 mmol of thioether was introduced into the mixture and stirred at room temperature for the specified duration. To recover both the product and any remaining reagents, the mixture was diluted with 1.5 mL of tetrahydrofuran (THF). The material was then separated through centrifugation, and the supernatant was collected and stored in a clean vial. For assessing the conversion and selectivity, a ¹H-NMR spectrum of the crude reaction was recorded in CDCl₃ solvent.

6.5. Recycling of GAA

The residual material from the reaction was retrieved using acetone and stored in a flask. Once a substantial amount of material had been accumulated, it was filtered

through a PTFE membrane (0.2 μm pore size), cleaned with acetone (3x50 mL), and left to dry on the filter overnight.

The following day, the material was collected from the filter and dispersed in Milli-Q water, followed by another filtration using a PC membrane (0.2 μm pore size). Subsequently, the material was washed with ethanol (3x50 mL) and then dispersed in the minimum possible amount of the same solvent.

6.6. General Procedure for Determining Hydrogen Peroxide Concentration via UV-Vis Absorbance of Titanyl Sulphate Complex

A mixture of GAA in Milli-Q water was placed inside a round-bottom flask. After 10 minutes of sonication, 30% hydrogen peroxide (H_2O_2) was added and stirred magnetically for the desired duration. Subsequently, the solution was diluted with Milli-Q water, which had been pre-acidified to pH 1-2 using 98% sulfuric acid, until the H_2O_2 concentration reached approximately 1 mM. To 10 mL of this solution, 0.5 mL of titanil sulfate was added, resulting in a yellow solution, which was then analyzed using a UV-Vis spectrometer in the range of 350-800 nm.

6.7. Analysis of Oxygen Evolution Using a NeoFox Oxygen Probe

A mixture of material was placed inside a three-necked round-bottom flask. Subsequently, all three necks were sealed with rubber plugs. The right and left plugs were perforated to allow for the insertion of entry and exit needles, respectively. The entry needle was connected to a nitrogen line, while the exit needle terminated inside a vial containing water.

The oxygen probe was inserted into the remaining neck, and the oxygen concentration inside the flask was reduced to nearly 0% using the nitrogen line. Subsequently, the entry needle was removed, and hydrogen peroxide was added using a syringe. The evolution of oxygen was then monitored for 30 minutes.

6.8. Additional NMR spectra

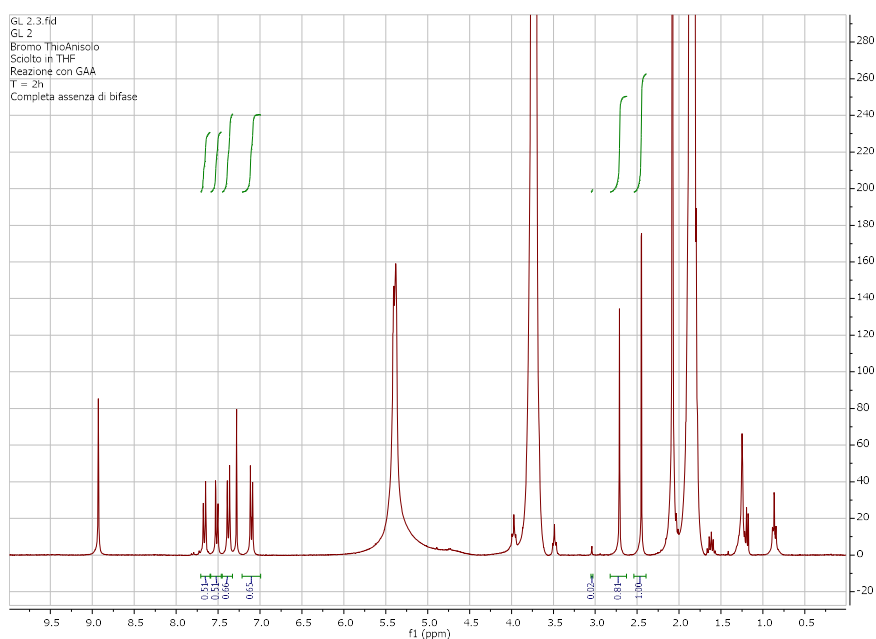


Figura 22: Bromothioanisole

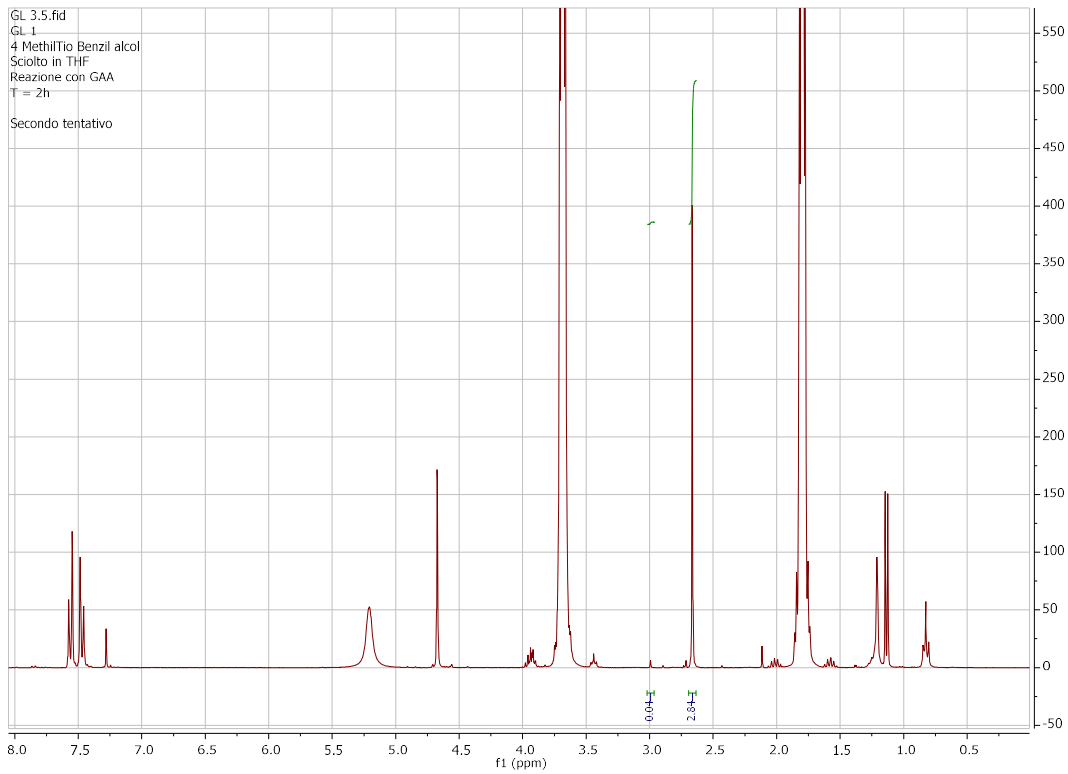


Figura 23: Methyltio benzil alcool

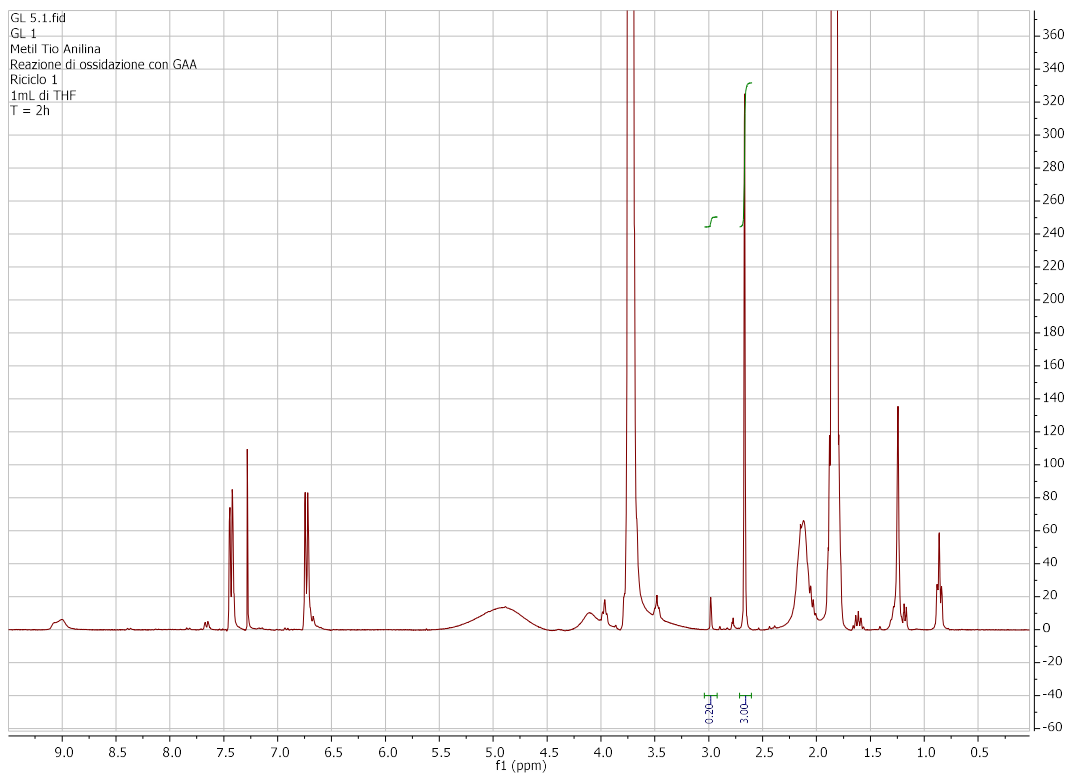


Figura 24: Methyltio anilina

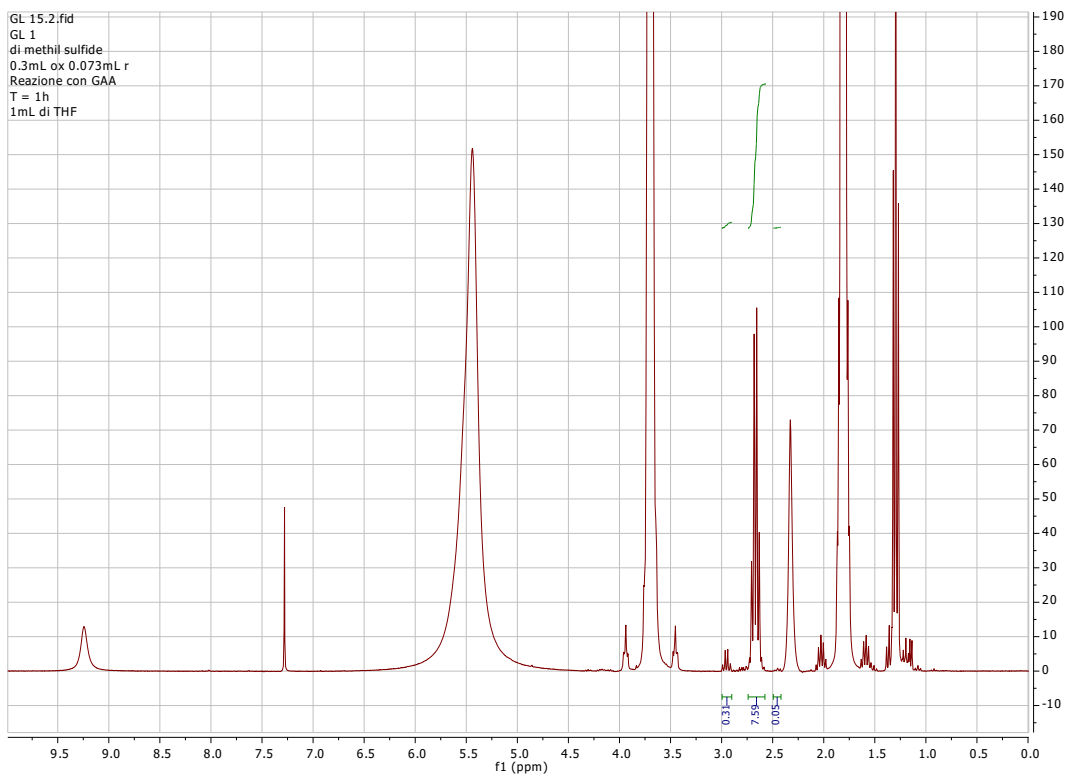
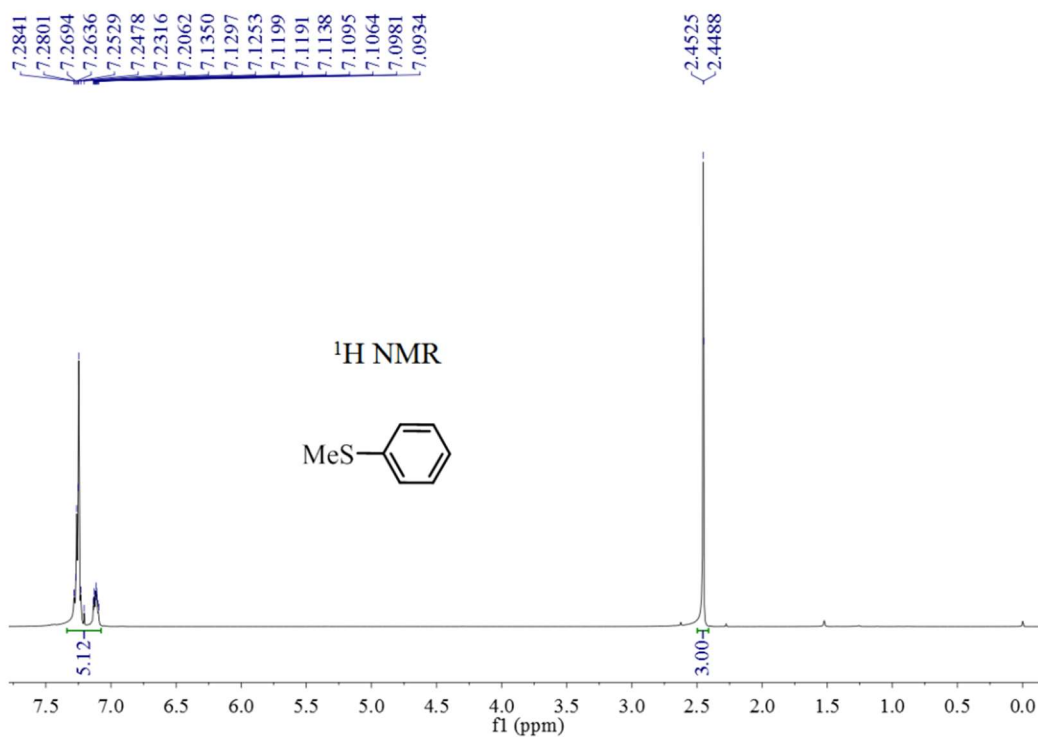
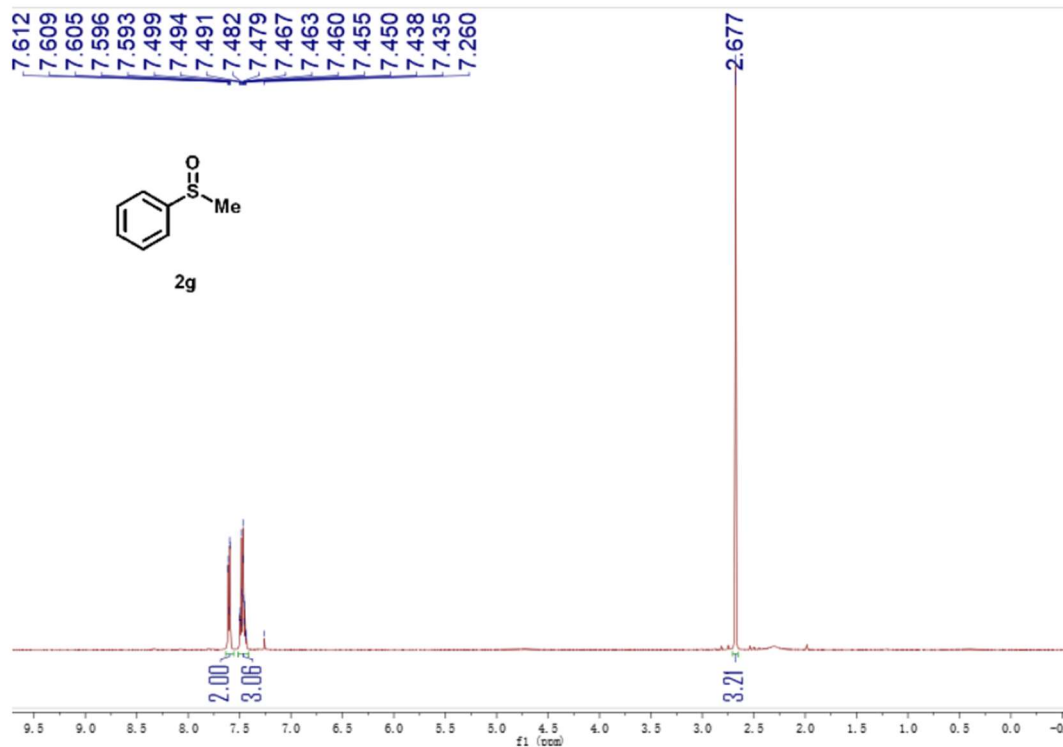


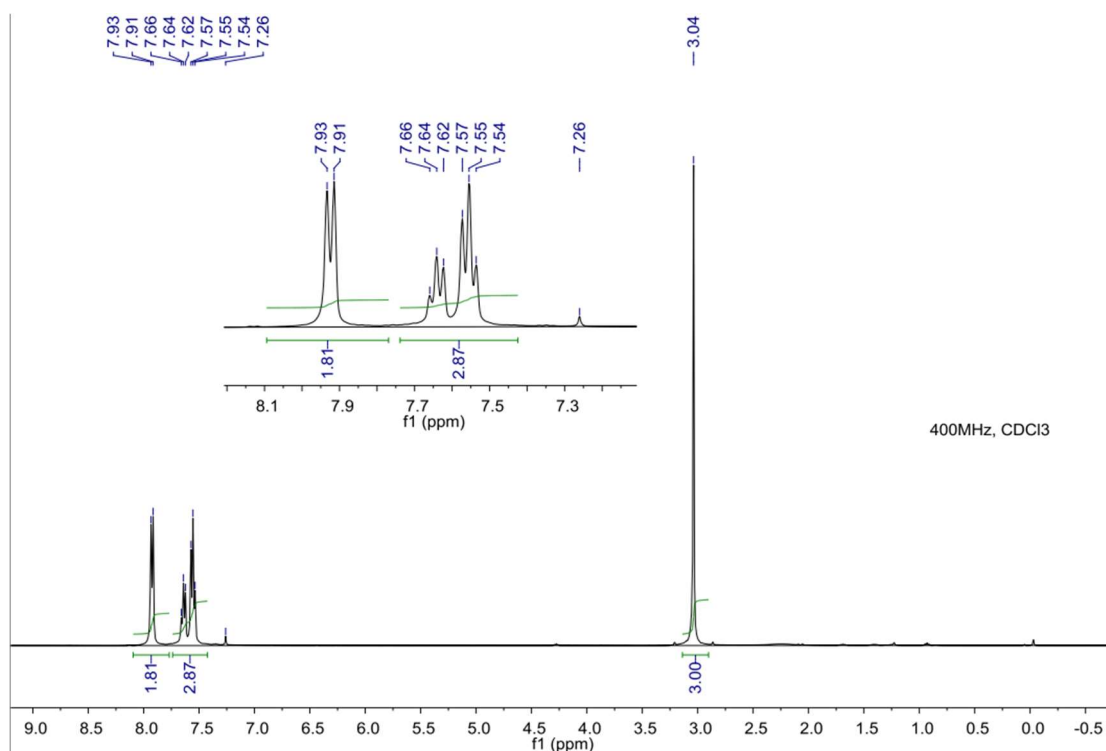
Figura 25: Diethyl sulfide



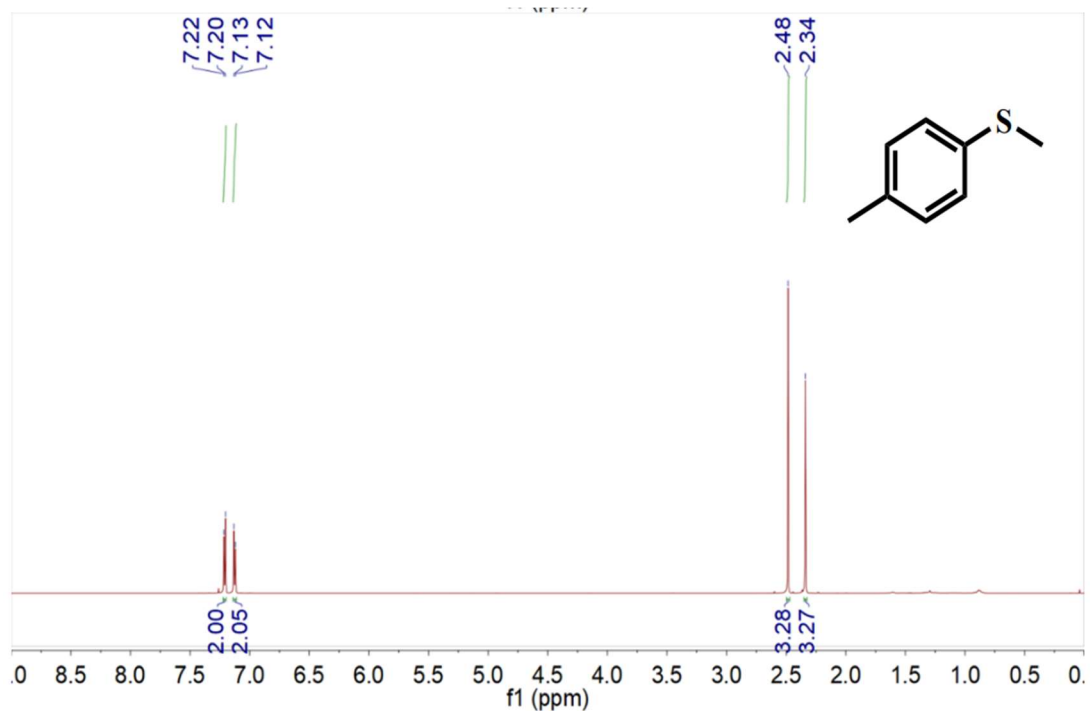
Methylthiobenzene ¹H NMR (400 MHz, CDCl₃): δ (ppm) 7.41–6.92 (m, 5H), 2.45 (d, J = 1.5 Hz, 3H).



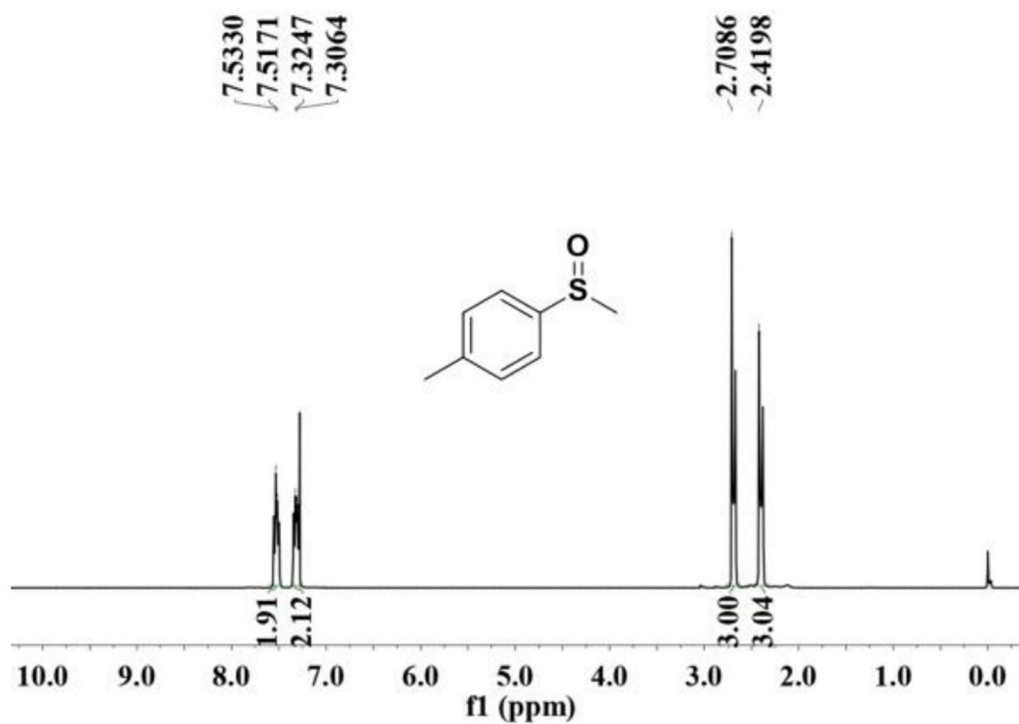
Methylphenyl sulfone ¹H NMR (500 MHz, CDCl₃) δ (ppm) 7.59–7.61 (m, 2H), 7.43–7.50 (m, 3H), 2.68 (s, 3H).



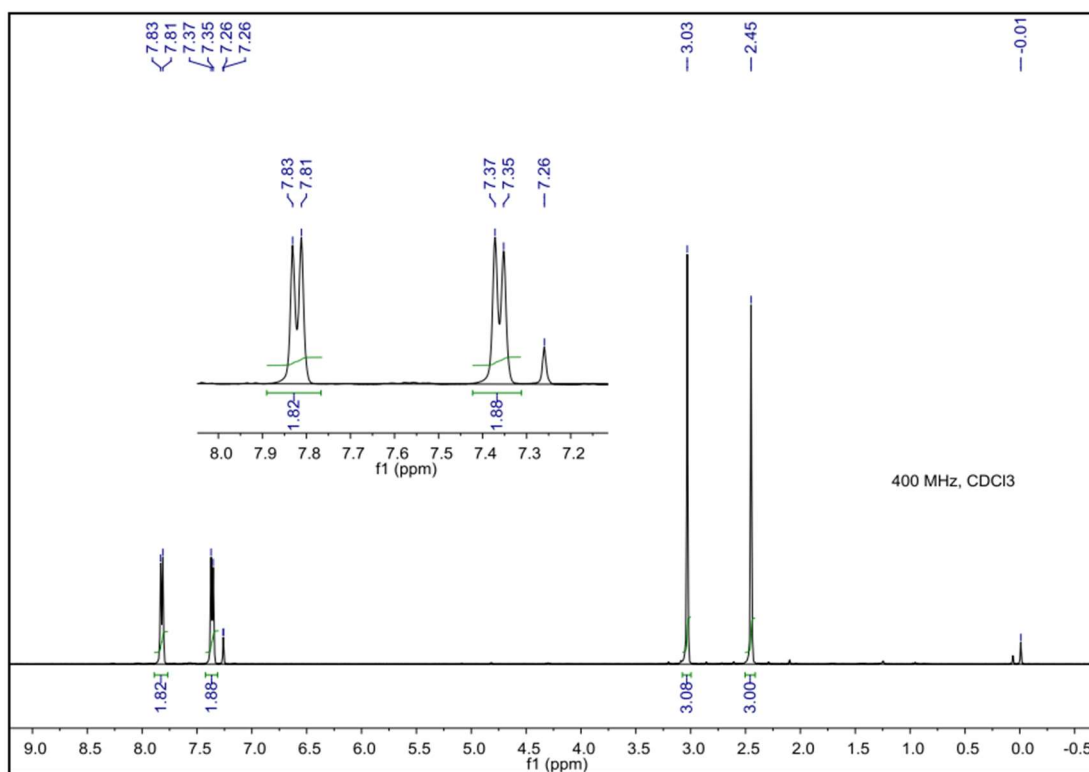
Phenyl methyl sulfone ¹H NMR (400 MHz, CDCl₃) δ (ppm): 7.92 (d, J = 7.5 Hz, 2H), 7.66–7.54 (m, 3H), 3.04 (s, 3H).



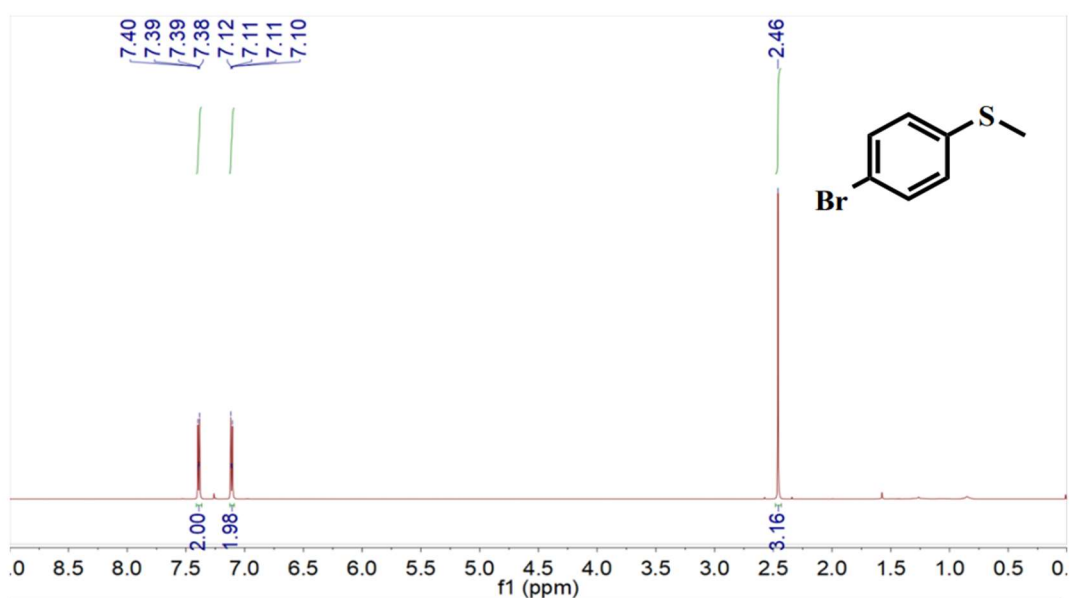
Methyl p-tolyl sulfide ^1H NMR (600 MHz, CDCl_3) δ 7.21 (d, $J = 8.2$ Hz, 2H), 7.13 (d, $J = 8.1$ Hz, 2H), 2.48 (s, 3H), 2.34 (s, 3H).



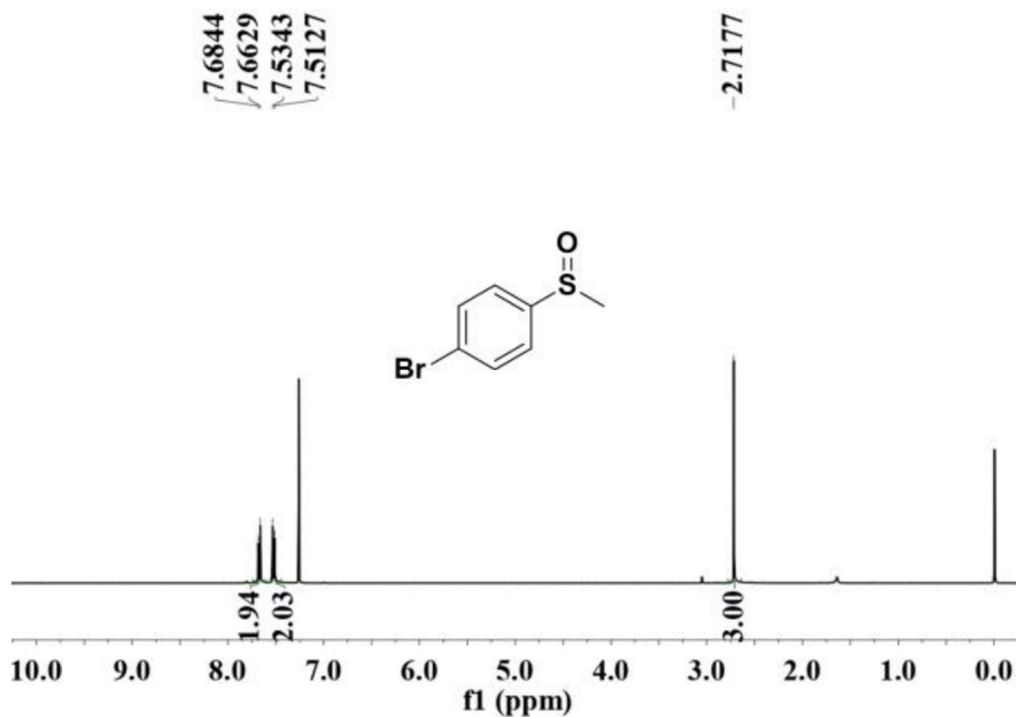
Methyl p-tolyl sulfoxide ^1H NMR (400 MHz, CDCl_3) δ 7.55-7.49 (m, 2H), 7.34-7.28 (m, 2H), 2.71 (s, 3H), 2.42 (s, 3H)



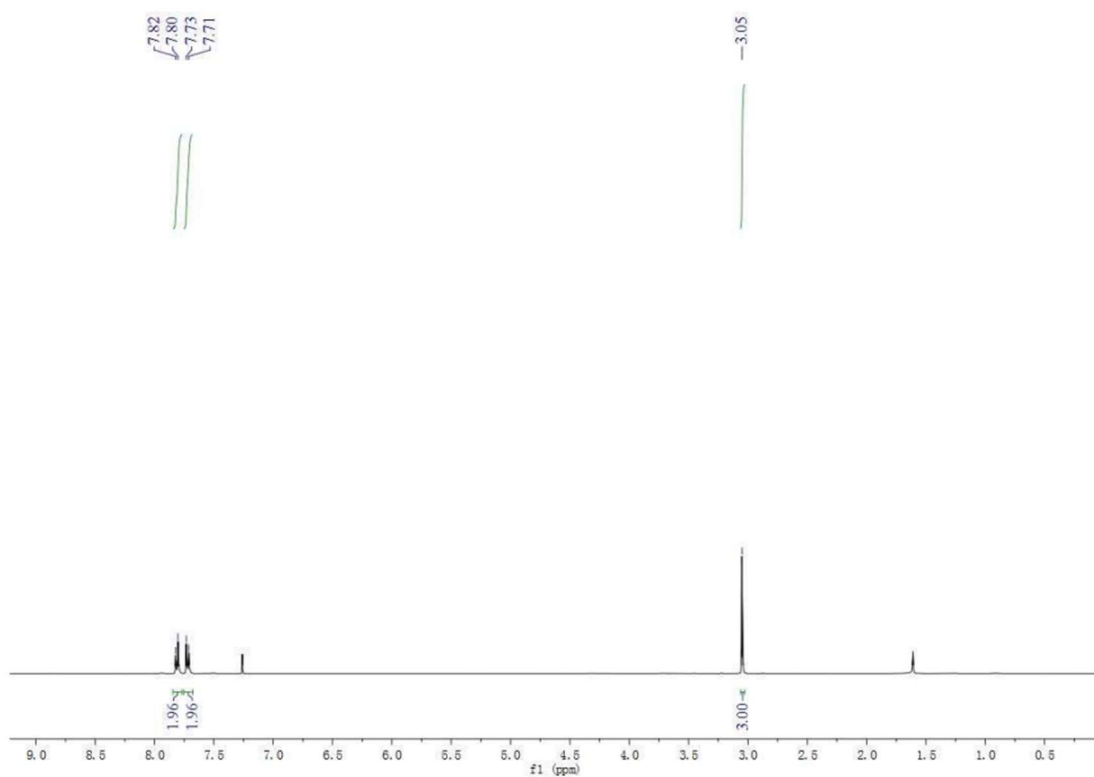
Methyl p-tolyl sulfone ¹H NMR (400 MHz, CDCl₃) δ (ppm): 7.82 (d, J = 8.0 Hz, 2H), 7.36 (d, J = 7.9 Hz, 2H), 3.03 (s, 3H), 2.45 (s, 3H)



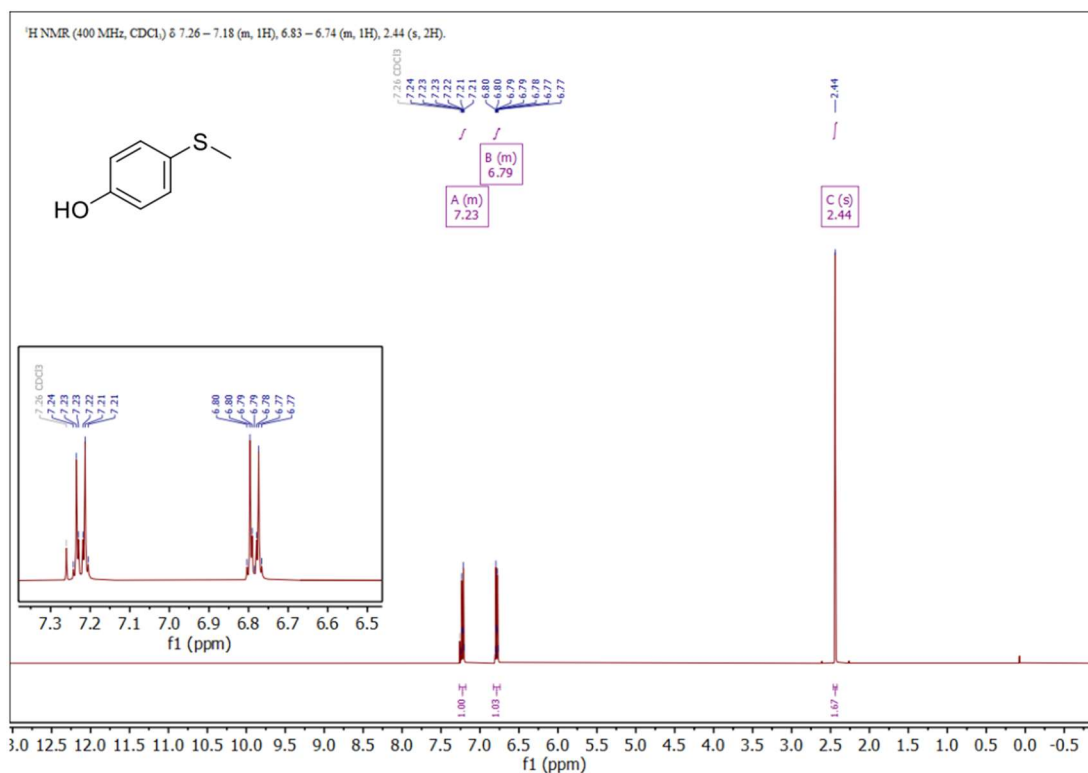
4-Bromo thioanisole ¹H NMR (600 MHz, CDCl₃) δ 7.41 – 7.37 (m, 2H), 7.13 – 7.09 (m, 2H), 2.46 (s, 3H).



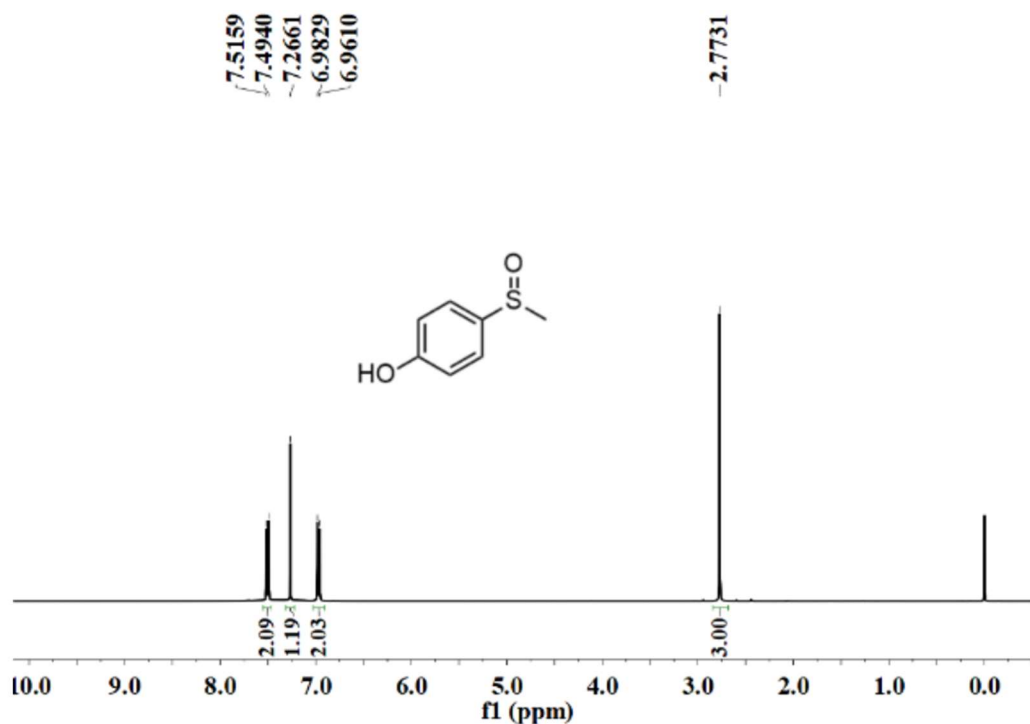
4 bromo methyl benzyl sulfoxide ^1H NMR (400 MHz, CDCl_3) δ 7.67 (d, $J = 8.6$ Hz, 2H), 7.52 (d, $J = 8.6$ Hz, 2H), 2.72 (s, 3H)



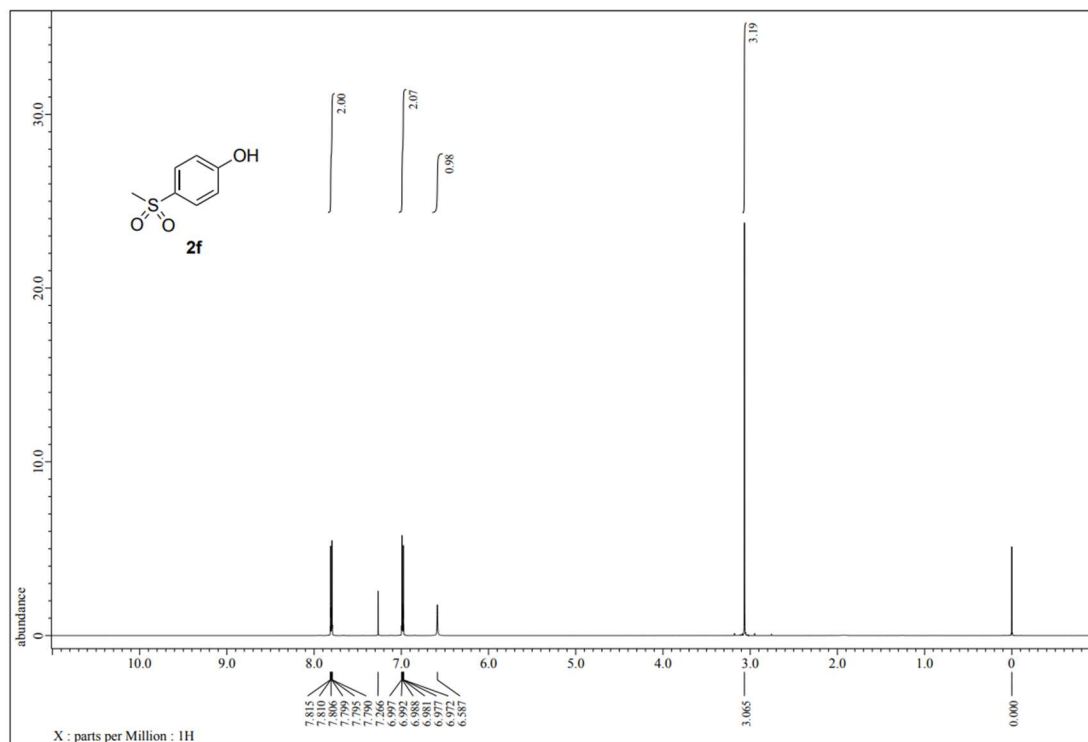
4 bromo methyl benzyl sulfide ^1H NMR (400 MHz, CDCl_3) δ 7.67 (d, $J = 8.4$ Hz, 2H), 7.52 (d, $J = 8.4$ Hz, 2H), 2.71 (s, 3H)



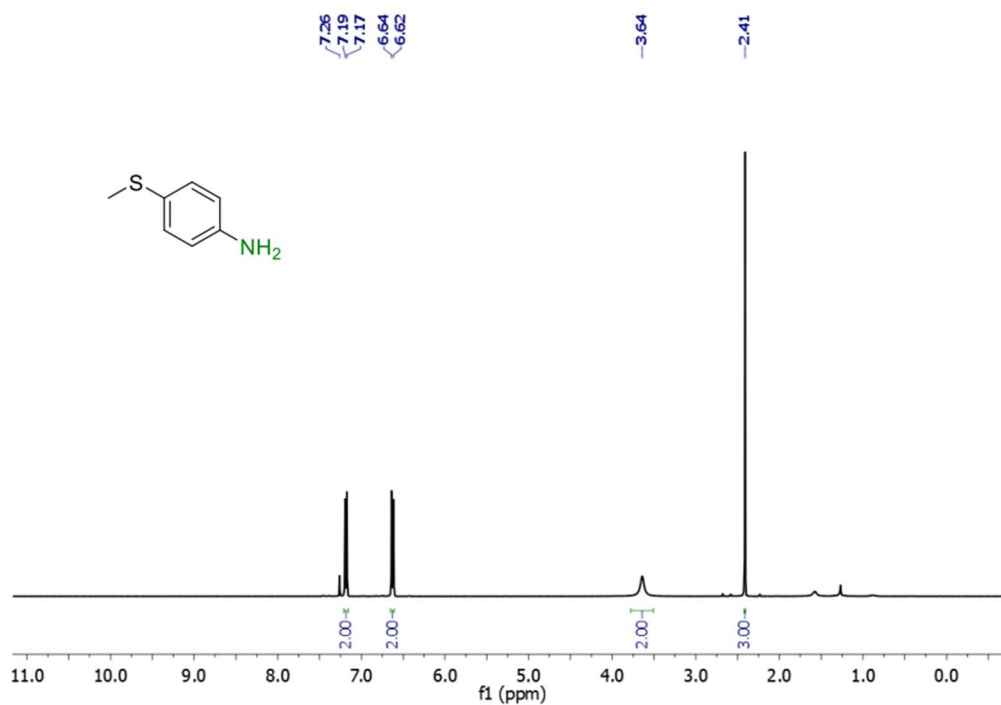
4 hydroxy thioanisole ¹H NMR (400 MHz, CDCl₃): δ = 7.26–7.18 (m, 2H), 6.83–6.74 (m, 2H), 2.44 (s, 3H) ppm.



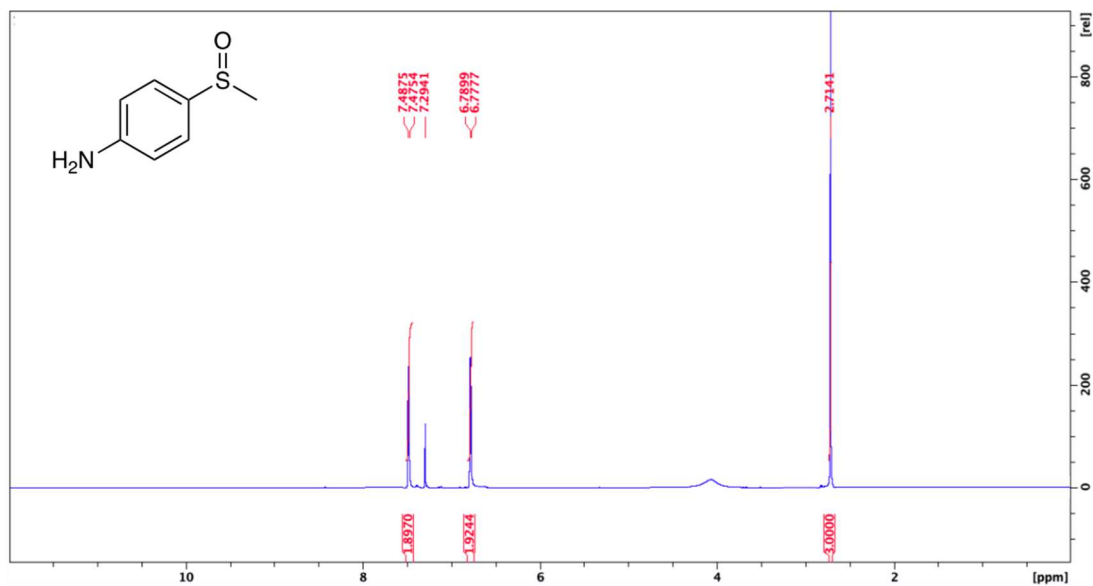
4 hydroxy methyl benzyl sulfoxide ¹H NMR (400 MHz, CDCl₃) δ 7.50 (d, J = 8.8 Hz, 2H), 7.27 (s, 1H), 6.97 (d, J = 8.8 Hz, 2H), 2.77 (s, 3H)



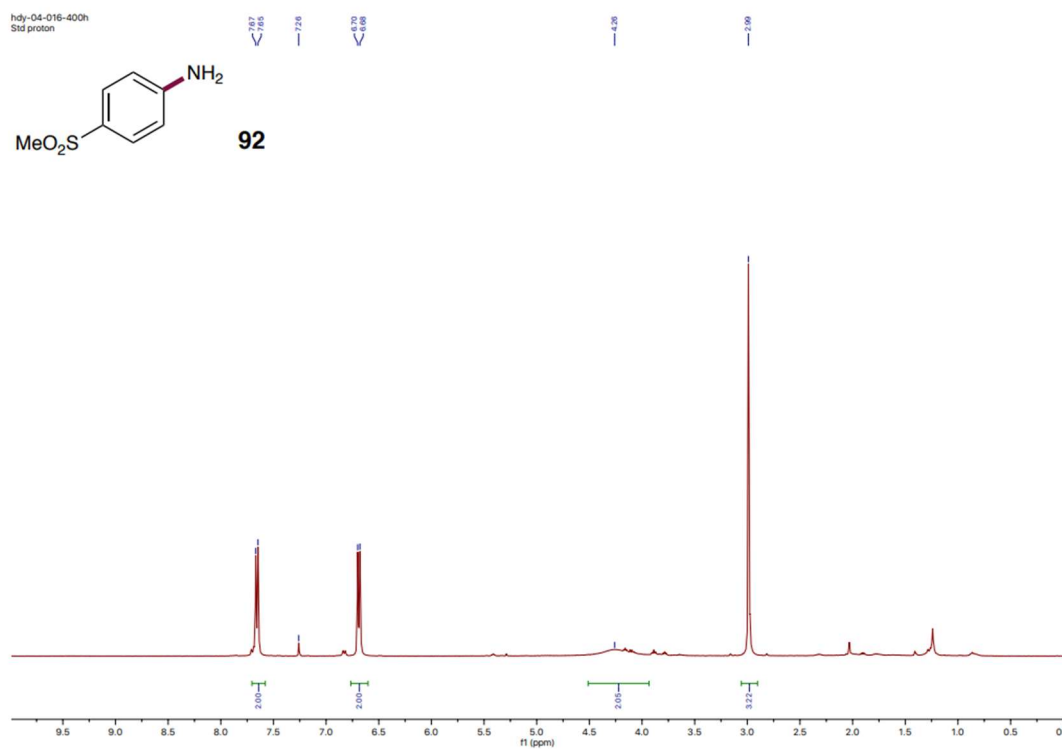
4 hydroxyl methyl benzyl sulfone ¹H NMR (600 MHz, CDCl₃, rt): d 7.82–7.79 (m, 2H), 7.00–6.97 (m, 2H), 6.59 (brs, 1H), 3.07 (s, 3H)



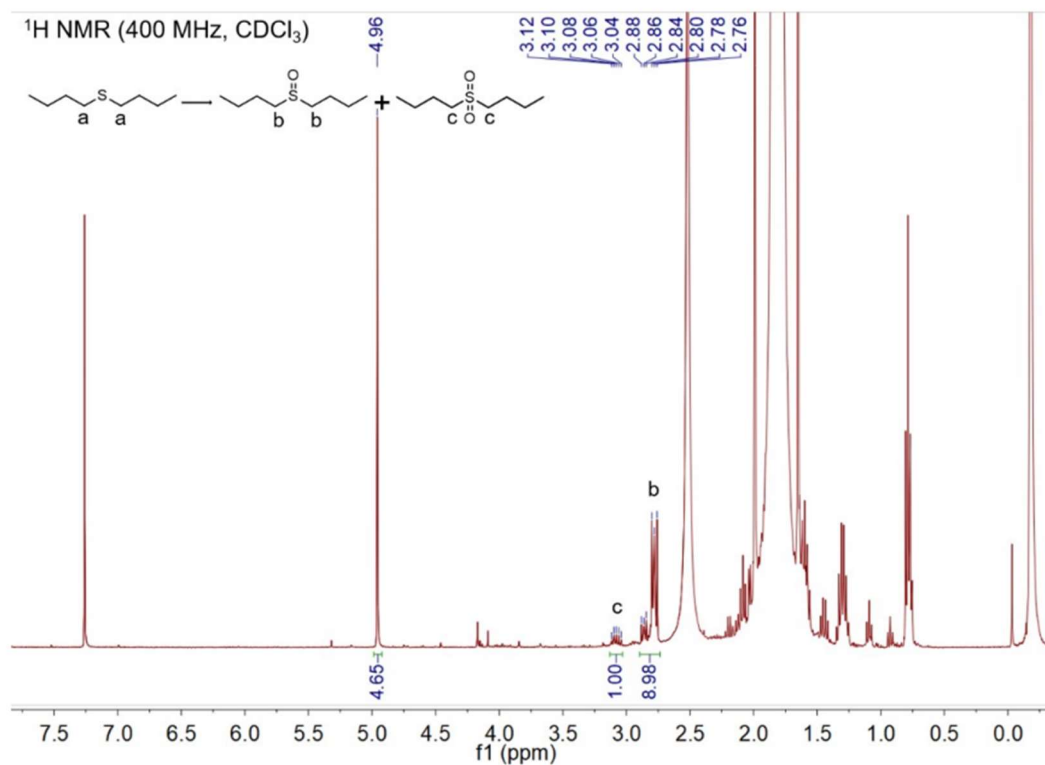
4 methyl thio aniline ¹H NMR (400 MHz, CDCl₃) δ 7.18 (d, J = 8.6 Hz, 2H), 6.63 (d, J = 8.5 Hz, 2H), 3.64 (brs, 2H), 2.41 (s, 3H).



4 amino methyl benzyl sulfoxide 1H NMR (500 MHz, CDCl₃): δ (ppm) 2.69 (3H, d, -CH₃), 3.63-4.11 (2H, br, -NH₂), 6.73-6.75 (2H, d, Ph-H), 7.42-7.44(2H, d, Ph-H)



4 ammino methyl benzyl sulfone 1H NMR (400 MHz, CDCl₃) δ 7.66 (d, J = 8.5 Hz, 2H), 6.69 (d, J = 8.5 Hz, 2H), 4.26 (br s, 2H), 2.99 (s, 3H)



Bibliography

1. Anastas, P. & Eghbali, N. Green Chemistry: Principles and Practice. *Chem. Soc. Rev* **39**, 301–312 (2010).
2. Molnár, Á. & Papp, A. Catalyst recycling-A survey of recent progress and current status. (2017) doi:10.1016/j.ccr.2017.08.011.
3. Leofanti, G., Padovan, M., Tozzola, G. & Venturelli, B. Surface area and pore texture of catalysts. *Catal Today* **41**, 207–219 (1998).
4. Machado Ab, B. F. & Serp, P. Graphene-based materials for catalysis. *This journal is Cite this: Catal. Sci. Technol* **2**, 54–75 (2012).
5. Directorate-General for Internal Market, I. E. and Sme. European Critical Raw Materials Act. *COM(2023) 160, SWD(2023) 160, SWD(2023) 161, SWD(2023) 162, SEC(2023) 360* https://single-market-economy.ec.europa.eu/publications/european-critical-raw-materials-act_en (2023).
6. L. Landau. ON THE THEORY OF PHASE TRANSITIONS. *Zh. Eksp. Teor.* **7**, 19–32 (1937).
7. Allen, M. J., Tung, V. C. & Kaner, R. B. Honeycomb Carbon: A Review of Graphene. (2006) doi:10.1021/cr900070d.

8. Hummers, W. S. & Offeman, R. E. Preparation of Graphitic Oxide. *J Am Chem Soc* **80**, 1339 (1958).
9. Ahmad, N., Kausar, A. & Muhammad, B. An investigation on 4-aminobenzoic acid modified polyvinyl chloride/graphene oxide and PVC/graphene oxide based nanocomposite membranes. *Journal of Plastic Film and Sheeting* **32**, 419–448 (2016).
10. Kiang Chua, C. & Pumera, M. Chemical reduction of graphene oxide: a synthetic chemistry viewpoint. *Chem. Soc. Rev* **43**, 291 (2014).
11. Novoselov, K. S. *et al.* A roadmap for graphene. *Nature* **490**, (2012).
12. Bai, H. *et al.* Functional Composite Materials Based on Chemically Converted Graphene. *Advanced Materials* **23**, 1089–1115 (2011).
13. Georgakilas, V. *et al.* Functionalization of graphene: Covalent and non-covalent approaches, derivatives and applications. *Chem Rev* **112**, 6156–6214 (2012).
14. Wang, H., Maiyalagan, T. & Wang, X. Review on recent progress in nitrogen-doped graphene: Synthesis, characterization, and its potential applications. *ACS Catal* **2**, 781–794 (2012).
15. Agnoli, S. & Favaro, M. Doping graphene with boron: a review of synthesis methods, physicochemical characterization, and emerging applications. *J Mater Chem A Mater* **4**, 5002–5025 (2016).
16. C Paulus, G. L., Hua Wang, Q. & Strano, M. S. Covalent Electron Transfer Chemistry of Graphene with Diazonium Salts. *Acc Chem Res* **46**, 160–170 (2013).
17. Giinther Tegge. Masthead. *Starch - Stärke* **39**, fmi-fmi (1987).
18. Medved', M. *et al.* Reactivity of fluorographene is triggered by point defects: beyond the perfect 2D world †. *Nanoscale* **10**, 4696 (2018).
19. Liang, Y. & Yang, L. Electronic structure and optical absorption of fluorographene. *Materials Research Society Symposium Proceedings* **1370**, 37–45 (2011).
20. Wang, X. *et al.* Controllable defluorination of fluorinated graphene and weakening of C-F bonding under the action of nucleophilic dipolar solvent †. *Phys. Chem. Chem. Phys* **18**, 3285 (2016).
21. Robinson, J. T. *et al.* Properties of Fluorinated Graphene Films. **10**, 6 (2010).
22. Matúš, M. *et al.* Reactivity of Fluorographene: A Facile Way toward Graphene Derivatives. (2015) doi:10.1021/acs.jpcclett.5b00565.
23. Chronopoulos, D. D. *et al.* High-Yield Alkylation and Arylation of Graphene via Grignard Reaction with Fluorographene. *Chem. Mater* **29**, 32 (2017).
24. Bakandritsos, A. *et al.* FULL PAPER www.afm-journal.de High-Performance Supercapacitors Based on a Zwitterionic Network of Covalently Functionalized Graphene with Iron Tetraaminophthalocyanine. (2018) doi:10.1002/adfm.201801111.

25. Bar, H. *et al.* Bimodal role of fluorine atoms in fluorographene chemistry opens a simple way toward double functionalization of graphene. (2019) doi:10.1016/j.carbon.2019.01.059.
26. Chronopoulos, D. D. *et al.* Alkynylation of graphene via the Sonogashira C-C cross-coupling reaction on fluorographene †. *This journal is Cite this: Chem. Commun* **55**, 1088 (2019).
27. Bakandritsos, A. *et al.* Cyanographene and Graphene Acid: Emerging Derivatives Enabling High-Yield and Selective Functionalization of Graphene. *ACS Nano* **11**, 58 (2017).
28. Ruff, O. & Bretschneider, O. Die Reaktionsprodukte der verschiedenen Kohlenstoffformen mit Fluor II (Kohlenstoff-monofluorid). *Z Anorg Allg Chem* **217**, 1–18 (1934).
29. Nair, R. R. *et al.* Fluorographene: a two-dimensional counterpart of Teflon. *Small* **6**, 2877–2884 (2010).
30. Lee, W. H. *et al.* Selective-area fluorination of graphene with fluoropolymer and laser irradiation. *Nano Lett* **12**, 2374–2378 (2012).
31. Olsavsky, N. J. *et al.* Research and Regulatory Advancements on Remediation and Degradation of Fluorinated Polymer Compounds. *Applied Sciences 2020, Vol. 10, Page 6921* **10**, 6921 (2020).
32. Jankovsky, O. *et al.* A New Member of the Graphene Family: Graphene Acid. *Chemistry A European Journal* **22**, 17416–17424 (2016).
33. Bakandritsos, A. *et al.* Cyanographene and Graphene Acid: Emerging Derivatives Enabling High-Yield and Selective Functionalization of Graphene. *ACS Nano* **11**, 46 (2017).
34. Blanco, M., Agnoli, S. & Granozzi, G. Graphene Acid: A Versatile 2D Platform for Catalysis. (2022) doi:10.1002/ijch.202100118.
35. Lerf, A., He, H., Forster, M. & Klinowski, J. Structure of graphite oxide revisited. *Journal of Physical Chemistry B* **102**, 4477–4482 (1998).
36. Abdi, G., Alizadeh, A. & Khodaei, M. M. Highly carboxyl-decorated graphene oxide sheets as metal-free catalytic system for chemoselective oxidation of sulfides to sulfones. *Mater Chem Phys* **201**, 323–330 (2017).
37. Khan, K. & Derindere Köse, S. Is palladium price in bubble? (2020) doi:10.1016/j.resourpol.2020.101780.
38. Dreyer, D. R., Jia, H. P. & Bielawski, C. W. Graphene Oxide: A Convenient Carbocatalyst for Facilitating Oxidation and Hydration Reactions. *Angewandte Chemie International Edition* **49**, 6813–6816 (2010).
39. Presolski, S. & Pumera, M. Graphene Oxide: Carbocatalyst or Reagent? *Angewandte Chemie International Edition* **57**, 16713–16715 (2018).
40. Matías Blanco, S. *et al.* Showcasing research from Professor Agnoli's laboratory As featured in: Combined high degree of carboxylation and electronic conduction in

graphene acid sets new limits for metal free catalysis in alcohol oxidation †. (2019) doi:10.1039/c9sc02954k.

41. Yadav, G. D., Mewada, R. K., Wagh, D. P. & Manyar, H. G. Catalysis Science & Technology MINI REVIEW Advances and future trends in selective oxidation catalysis: a critical review. *Cite this: Catal. Sci. Technol* **12**, 7245 (2022).
42. Ali, M. E., Rahman, M. M., Sarkar, S. M., Bee, S. & Hamid, A. Heterogeneous Metal Catalysts for Oxidation Reactions. (2014) doi:10.1155/2014/192038.
43. Duan, X., Sun, H. & Wang, S. Metal-Free Carbocatalysis in Advanced Oxidation Reactions. *Acc Chem Res* **51**, 678–687 (2018).
44. Sun, H. *et al.* Reduced graphene oxide for catalytic oxidation of aqueous organic pollutants. *ACS Appl Mater Interfaces* **4**, 5466–5471 (2012).
45. Wang, Y., Ao, Z., Sun, H., Duan, X. & Wang, S. Activation of peroxymonosulfate by carbonaceous oxygen groups: experimental and density functional theory calculations. *Appl Catal B* **198**, 295–302 (2016).
46. Jiang, D. E., Sumpter, B. G. & Dai, S. Unique chemical reactivity of a graphene nanoribbon's zigzag edge. *Journal of Chemical Physics* **126**, (2007).
47. Duan, X. *et al.* Nitrogen-doped graphene for generation and evolution of reactive radicals by metal-free catalysis. *ACS Appl Mater Interfaces* **7**, 4169–4178 (2015).
48. Lee, H. *et al.* Activation of Persulfates by Graphitized Nanodiamonds for Removal of Organic Compounds. *Environ Sci Technol* **50**, 10134–10142 (2016).
49. Rekhate, C. V & Srivastava, J. K. Recent advances in ozone-based advanced oxidation processes for treatment of wastewater-A review. *Chemical Engineering Journal Advances* **3**, 100031 (2020).
50. Ciriminna, R., Albanese, L., Meneguzzo, F. & Pagliaro, M. Hydrogen Peroxide: A Key Chemical for Today's Sustainable Development. *ChemSusChem* **9**, 3374–3381 (2016).
51. Lenz, R. W., Handlovits, C. E. & Smith, H. A. Phenylene sulfide polymers. III. The synthesis of linear polyphenylene sulfide. *Journal of Polymer Science* **58**, 351–367 (1962).
52. Masdeu-Bultó, A. M., Diéguez, M., Martín, E. & Gómez, M. Chiral thioether ligands: coordination chemistry and asymmetric catalysis. *Coord Chem Rev* **242**, 159–201 (2003).
53. Hashmi, M. P. & Koester, T. M. Applications of Synthetically Produced Materials in Clinical Medicine. *Reference Module in Materials Science and Materials Engineering* (2018) doi:10.1016/B978-0-12-803581-8.10258-9.
54. Jan-Erling Bäckvall. *Modern Oxidation Methods. Modern Oxidation Methods* (Wiley, 2004). doi:10.1002/3527603689.
55. Xie, F. *et al.* Thioanisole oxidation with hydrogen peroxide catalyzed by hexadentate 8-quinolinolato manganese(III) complexes. *J Mol Catal A Chem* **307**, 93–97 (2009).

56. Riemke, F. C. *et al.* Influence of Nb₂O₅ grown on SrTiO₃ nanoseeds in the catalytic oxidation of thioanisole. *Mater Chem Phys* **278**, 125591 (2022).
57. Golchoubian, H. & Hosseinpoor, F. Effective Oxidation of Sulfides to Sulfoxides with Hydrogen Peroxide under Transition-Metal-Free Conditions. *Molecules* **2007**, Vol. *12*, Pages 304-311 **12**, 304–311 (2007).
58. Marcano, D. C. *et al.* Improved synthesis of graphene oxide. *ACS Nano* **4**, 4806–4814 (2010).
59. Aruoma, O. I. & Halliwell, Barry. Molecular biology of free radicals in human diseases. 430 (1998).
60. Winterbourn, C. C. The Biological Chemistry of Hydrogen Peroxide. *Methods Enzymol* **528**, 3–25 (2013).
61. Tkaczyk, C. *et al.* Significance of Elevated Blood Metal Ion Levels in Patients with Metal-on-Metal Prostheses: An Evaluation of Oxidative Stress Markers. *Open Orthop J* **4**, 221 (2010).
62. Rinnerthaler, M., Bischof, J., Streubel, M. K., Trost, A. & Richter, K. Oxidative Stress in Aging Human Skin. *Biomolecules* **2015**, Vol. *5*, Pages 545-589 **5**, 545–589 (2015).
63. Liguori, I. *et al.* Oxidative stress, aging, and diseases. *Clin Interv Aging* **13**, 757–772 (2018).
64. Pędziwiatr, P. *et al.* RIC Pro-Akademia-CC BY DECOMPOSITION OF HYDROGEN PERODIXE-KINETICS AND REVIEW OF CHOSEN CATALYSTS. *Acta Innovations* 45–52 (2018) doi:10.32933/ActaInnovations.26.5.
65. Alfonso-Prieto, M., Biarnés, X., Vidossich, P. & Rovira, C. The molecular mechanism of the catalase reaction. *J Am Chem Soc* **131**, 11751–11761 (2009).
66. Henderson, R. K. *et al.* Expanding GSK’s solvent selection guide – embedding sustainability into solvent selection starting at medicinal chemistry. *Green Chemistry* **13**, 854–862 (2011).
67. Yeh, J. J. & Lindau, I. Atomic subshell photoionization cross sections and asymmetry parameters: $1 \leq Z \leq 103$. *At Data Nucl Data Tables* **32**, 1–155 (1985).
68. Shinotsuka, H., Tanuma, S., Powell, C. J. & Penn, D. R. Calculations of electron inelastic mean free paths. X. Data for 41 elemental solids over the 50 eV to 200 keV range with the relativistic full Penn algorithm. *Surface and Interface Analysis* **47**, 1132–1132 (2015).
69. Gupta, B. *et al.* Role of oxygen functional groups in reduced graphene oxide for lubrication. *Sci Rep* **7**, (2017).
70. Stobinski, L. *et al.* Graphene oxide and reduced graphene oxide studied by the XRD, TEM and electron spectroscopy methods. *J Electron Spectros Relat Phenomena* **195**, 145–154 (2014).
71. Yang, Y., Lu, G., Li, Y., Liu, Z. & Huang, X. One-Step Preparation of Fluorographene: A Highly Efficient, Low-Cost, and Large-Scale Approach of Exfoliating Fluorographite. (2013) doi:10.1021/am405046u.

72. Dreyer, D. R., Jia, H. P., Todd, A. D., Geng, J. & Bielawski, C. W. Graphite oxide: a selective and highly efficient oxidant of thiols and sulfides. *Org Biomol Chem* **9**, 7292–7295 (2011).
73. Sarkar, A. *et al.* A decade update on solvent and catalyst-free neat organic reactions: a step forward towards sustainability. *Green Chemistry* **18**, 4475–4525 (2016).
74. Riemke, F. C. *et al.* Influence of Nb₂O₅ grown on SrTiO₃ nanoseeds in the catalytic oxidation of thioanisole. *Mater Chem Phys* **278**, 125591 (2022).
75. Li, W., Xie, Z. & Jing, X. BODIPY photocatalyzed oxidation of thioanisole under visible light. *Catal Commun* **16**, 94–97 (2011).
76. Tshentu, Z. R., Togo, C. & Walmsley, R. S. Polymer-anchored oxovanadium(IV) complex for the oxidation of thioanisole, styrene and ethylbenzene. *J Mol Catal A Chem* **318**, 30–35 (2010).
77. Scott, K. A. & Njardarson, J. T. Analysis of US FDA-Approved Drugs Containing Sulfur Atoms. *Top Curr Chem (Z)* **376**, 5 (2018).